Organolanthanide-Catalyzed Hydroamination. A Kinetic, Mechanistic, and Diastereoselectivity Study of the Cyclization of N-Unprotected Amino Olefins

Michel R. Gagné, Charlotte L. Stern, and Tobin J. Marks*

Contribution from the Department of Chemistry, Northwestern University, Evanston, Illinois 60208. *Received June 24, 1991*

Abstract: This contribution reports the efficient, regiospecific Cp'_2LnR [Cp' = η^5-Me_5C_5; R = H, $CH(TMS)_2$, η^3-C_3H_5, $N(TMS)_2$; Ln = La, Nd, Sm, Y, Lu]-catalyzed hydroamination/cyclization of the amino olefins $H_2NCHR^1R^2CH{=}CH_2$ to yield the corresponding heterocycles $HNCH(R^1)R^2CHCH_3$, where R^1, R^2, N_t (turnover frequency, h^{-1}), °C: H, $(CH_2)_2$, 140, 60 °C; H, CMe_2CH_2, 95, 25 °C; H, $(CH_2)_3$, 5, 60 °C; CH_3, $(CH_2)_2$, 45, 25 °C; H, CH(Me)CH_2, 38, 25 °C; and *o*-C_6H_4, CH_2, 13, 80 °C. In addition, $Me_2Si(Me_4C_5)_2NdCH(TMS)_2$ effects the cyclization of $CH_3HN(CH_2)_3CH{=}CH_2$ and $H_2NCH_2CMe_2(CH_2)_3CH{=}CH_2$ with N_t = 11 h^{-1} (25 °C) and 0.3 h^{-1} (60 °C), respectively. Reactions are zero-order in substrate over 3 or more half-lives, and for the cyclization of $H_2N(CH_2)_3CH{=}CH_2$ by catalyst precursor $Cp'_2LaCH(TMS)_2$, $\Delta H^{\ddagger}$ = 12.7 (1.4) kcal mol^{-1} and $\Delta S^{\ddagger}$ = −27 (5) eu. Kinetic isotope effects (k_H/k_D) of 2.7 (4) (60 °C), 5.2 (8) (25 °C), and 4.1 (8) (25 °C) are observed for the $Cp'_2LaCH(TMS)_2$-induced cyclizations of $D_2N(CH_2)_3CH{=}CH_2$, $D_2NCH(CH_3)(CH_2)_2CH{=}CH_2$, and $D_2NCH_2C(CH_3)_2CH_2CH{=}CH_2$, respectively. Cyclization yields the corresponding $DNCH(R^1)R^2CHCH_2D$ isotopomers exclusively. Cyclization of $H_2NCH_2C(CH_3)_2CH_2CH{=}CH_2$ by catalyst precursor $Cp'_2LaCH(TMS)_2$ exhibits the solvent effect, $k_{toluene}/k_{THF}$ = 5.3 (5). The complexes $Cp'_2LnNHR(H_2NR)$ (Ln = La, R = CH_3, CH_2CH_3; Ln = Nd, R = CH_2CH_3) and $Cp'_2LaNCH(CH_3)CH_2CR_2CH_2(HNCH(CH_3)CH_2CR_2CH_2)$ (R = H, CH_3) were synthesized to model species in the catalytic cycle. Crystallographic data for $Cp'_2LaNHCH_3(H_2NCH_3)$ at −120 °C were as follows: $P2_1/n$, Z = 4, a = 19.901 (4) Å, b = 11.695 (3) Å, c = 20.202 (3) Å, β = 97.95 (2)°, and $R(F)$ = 0.049 for 3296 independent reflections with $I > 2.58\sigma(I)$. Two independent molecules crystallize per unit cell with average La–$NHCH_3$ and La←NH_2CH_3 bond distances of 2.31 (1) and 2.70 (1) Å, respectively. The two molecules differ slightly in relative orientations of the NCH_3 groups. The amine–amido complexes undergo rapid intramolecular proton transfer between amine and amido ligands ($\Delta G^{\ddagger} \approx 12.4 \pm 0.5$ kcal mol^{-1}). Intermolecular exchange with free amine is rapid on the NMR time scale at −80 °C. The ordering of precatalyst activities, $(Cp'_2LaCH(TMS)_2 > Cp'_2SmCH(TMS)_2 > Cp'_2LuCH(TMS)_2$; $Et_2Si(C_5H_4)(Me_4C_5)LuCH(TMS)_2 > Me_2Si(Me_4C_5)_2LuCH(TMS)_2 > Cp'_2LuCH(TMS)_2)$ accords with known olefin insertion reactivities. Diastereoselection in $H_2NCH(CH_3)(CH_2)_2CH{=}CH_2$ (**5**) cyclization depends on both lanthanide and ancillary ligation. Final 2,5-dimethylpyrrolidine trans:cis ratios in L_nLnR-catalyzed reactions for L_n, Ln, trans:cis, °C are as follows: Cp'_2, La, 3:2, 50 °C; Cp'_2, La, 5:1, 25 °C; Cp'_2, La, 8:1, 0 °C; Cp'_2, Nd, 1:1.25, 25 °C; Cp'_2, Sm, 1:1.25, 25 °C; Cp'_2, Y, 8:1, 25 °C; $Me_2Si(Me_4C_5)_2$, Y, 3:1, 25 °C; $Et_2Si(H_4C_5)(Me_4C_5)$, Y, 18:1, 25 °C; $Et_2Si(H_4C_5)(Me_4C_5)$, Lu, 4:1, 25 °C. For the $Cp'_2LaCH(TMS)_2$-catalyzed case, the trans:cis ratio is also dependent on the extent of conversion and initial substrate:catalyst ratio. In contrast to **5**, $\mathbf{5d_2}$ exhibits low diastereoselectivity which is independent of conversion. In the presence of 3 equiv of *n*-propylamine, the $Cp'_2LaCH(TMS)_2$-catalyzed cyclization of **5** affords a ≥50:1 trans:cis product ratio. Mechanistic evidence suggests that olefin insertion into the Ln–N bond of the amine–amido complexes is turnover-limiting and is followed by a rapid protonolysis of the resulting Ln–C bond. The proposed catalytic mechanism invokes parallel manifolds, with one manifold populated at high amine concentrations exhibiting high diastereoselectivity in the cyclization of **5**, and with the second, favored at low substrate concentrations, exhibiting lower diastereoselectivity. The catalyst at high amine concentrations is postulated to be a Ln(amido)$(amine)_2$ complex.

Introduction

The use of early transition metal and f-element complexes to effect synthetically useful organic transformations is rapidly becoming an important interfacial boundary between traditional organometallic and synthetic organic chemistry.[1] A substantial amount of literature has recently emerged concerning stoichiometric activation of, and C–C bond formation involving, synthons such as alkynes,[2] benzynes,[3] alkenes,[4] imines,[5] and nitriles.[5] A largely unexplored area concerns the use of early transition metal complexes to catalyze the formation of carbon–heteroatom bonds.[1] For example, nitrogen-based molecules represent an important class of structures which pervade all of organic chemistry, and efficient new routes (especially catalytic) to such molecules would be of great interest.

Olefin hydroamination, which constitutes in a formal sense the addition of an N–H bond across a C=C bond, is a transformation of seemingly fundamental simplicity (eq 1) and would appear to offer an attractive route to numerous classes of organonitrogen molecules. However, efforts to effect such transformations

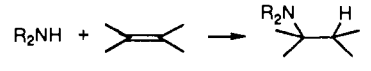

(1)

(1) For some leading review references, see: (a) Molander, G. A. In *The Chemistry of the Metal-Carbon Bond*; Hartley, F. R., Ed.; John Wiley Ltd: London, 1989; Vol. 5, Chapter 8. (b) McMurry, J. E. *Chem. Rev.* **1989**, *89*, 1513–1524. (c) Buchwald, S. L.; Nielsen, R. B. *Chem. Rev.* **1988**, *88*, 1047–1058. (d) Collman, J. P.; Hegedus, L. S.; Norton, J. R.; Finke, R. G. *Principles and Applications of Organotransition Metal Chemistry*; University Science Books: Mill Valley, CA, 1987; Part III. (e) Reetz, M. T. *Organotitanium Reagents in Organic Synthesis*; Springer-Verlag: Berlin, 1986. (f) Kagan, H. B. In *Fundamental and Technological Aspects of Organo-f-Element Chemistry*; Marks, T. J., Fragalà, I. L., Eds.; Reidel: Dordrecht, The Netherlands, 1985; Chapter 2. (g) Schwartz, J.; Labinger, J. A. In *New Synthetic Methods*; Verlag Chemie: New York, 1979; Vol. 5.

(2) (a) Takagi, K.; Rousset, C. J.; Negishi, E. *J. Am. Chem. Soc.* **1991**, *113*, 1440–1442. (b) Hartung, J. B., Jr.; Pedersen, S. F. *J. Am. Chem. Soc.* **1989**, *111*, 5468–5469. (c) Vaughan, G. A.; Hillhouse, G. L.; Reingold, A. L. *J. Am. Chem. Soc.* **1990**, *112*, 7994–8001. (d) Rajan Babu, T. V.; Nugent, W. A.; Taber, O. F.; Fagan, P. J. *J. Am. Chem. Soc.* **1988**, *110*, 7128–7135.

(3) Buchwald, S. L.; King, S. M. *J. Am. Chem. Soc.* **1991**, *113*, 258–265 and references therein.

(4) (a) Buchwald, S. L.; Fisher, R. A. *Organometallics* **1990**, *9*, 871–873 and references therein. (b) Buchwald, S. L.; Kreutzer, K. A.; Fisher, R. A. *J. Am. Chem. Soc.* **1990**, *112*, 4600–4601.

(5) (a) Roskamp, E. J.; Pedersen, S. F. *J. Am. Chem. Soc.* **1987**, *109*, 3152–3154. (b) Roskamp, E. J.; Pedersen, S. F. *J. Am. Chem. Soc.* **1987**, *109*, 6551–6553.

0002-7863/92/1514-275$03.00/0

catalytically in a general and efficient manner have met with only limited success.[6-9] Although eq 1 is exergonic for many simple amine/olefin pairs,[10] industrial-scale syntheses of alkylamines are usually achieved via dehydration of alcohols in the presence of amines. The alcohols in turn are usually produced via hydration of olefins.[11] Two basic approaches have been employed to effect eq 1 directly and involve primarily either olefin or amine activation routes. Olefin activation is generally accomplished with late transition metal catalysts, which polarize coordinated olefins and render them more susceptible to attack by exogenous amine nucleophiles.[6a,c,12] Solid acids have also been shown to catalyze eq 1 at high temperatures and pressures, presumably through carbocation intermediates.[13] The most widely employed amine activation approach utilizes alkali and alkaline earth metals to generate highly nucleophilic amido species, which then add to olefins.[8a] An alternative amine activation route employs an Ir(I) catalyst[7b] and NH oxidative activation to generate an Ir–N bond. When coupled to an olefin insertion/reductive elimination process, a cycle for olefin hydroamination is realized.[14]

Organolanthanide complexes of the type Cp'_2LnR ($Cp' = \eta^5$-Me_5C_5; R = H, $CH(TMS)_2$; Ln = La, Nd, Sm, Y, Lu) have been shown to be highly reactive with respect to olefin insertion processes (e.g., $N_t \gtrsim 1500\ s^{-1}$ for ethylene polymerization by Cp'_2La centers at 25 °C, 1 atm ethylene).[15,16] That this metal–ligand array supports olefin insertion into Ln–C and Ln–H bonds (eqs 2 and 3) with such extraordinary kinetic facility suggests that this may be an ideal environment in which to effect heretofore unrealized olefin insertion processes such as those involving metal–N bonds (eq 4).[17,18] Additionally, thermochemical data suggest that eq 4 is approximately thermoneutral,[19,20] and when coupled to the exothermic[19,20] (and kinetically facile[21]) protonolysis of eq 5, offers a potential catalytic pathway for organolanthanide-catalyzed olefin hydroamination. Literature precedent[12] and entropic considerations suggested that intramolecular approaches to olefin hydroamination, as shown in Scheme I, offered the greatest promise for initial investigation. Indeed, such an approach was successful as described in an earlier communication on the first catalytic hydroamination/cyclization of unprotected amino olefins.[22] In this contribution we now present a full discussion of the reaction scope, substrate selectivities, kinetics, and mechanism of this new catalytic process.

$$MCH_2R + CH_2{=}CH_2 \rightarrow MCH_2CH_2CH_2R \quad (2)$$

$$MH + CH_2{=}CHR \rightarrow MCH_2CH_2R \quad (3)$$

$$MNR_2 + CH_2{=}CHR' \xrightarrow{?} MCH_2CHR'NR_2 \quad (4)$$

$$LnCH_2R + HNR_2 \rightarrow LnNR_2 + CH_3R \quad (5)$$

Experimental Section

General Considerations. Manipulations of organolanthanide complexes were carried out either under an atmosphere of argon using standard high-vacuum techniques or in a Vacuum Atmospheres glovebox. Solvents used were predried and freshly distilled from Na/K alloy. Toluene-d_8 and tetrahydrofuran-d_8 (Cambridge Isotopes) used for NMR kinetic measurements were stored over Na/K alloy and vacuum-transferred immediately prior to use. Deuterium oxide was purchased from Cambridge Isotopes. All organic starting materials were purchased from Aldrich Chemical Co. and, when appropriate, were distilled or recrystallized prior to use. NMR spectra were recorded on a JEOL FX-270 (270 MHz ^{1}H; 67.80 MHz ^{13}C) or a Varian XL-400 (400 MHz ^{1}H; 100 MHz ^{13}C) spectrometer. Chemical shifts are reported relative to $SiMe_4$. IR spectra of liquid organic materials were recorded neat on KBr plates and those of organometallic compounds as Nujol mulls. Spectra were recorded on a Perkin-Elmer 283 spectrophotometer and calibrated with polystyrene film. GC/MS studies were performed on a VG70-250 SE instrument with 70-eV electron impact ionization. We thank Dr. Doris Hung for assistance. Cryoscopic molecular weight measurements were performed in a modified Knauer apparatus calibrated with $Cp'_2LaCH(TMS)_2$.

Reagents. Pentamethylcyclopentadiene was synthesized according to a procedure developed in this laboratory.[23] The compounds 2,2-dimethyl-1-aminopent-4-ene (**9**),[12a] 2-aminohex-5-ene (**5**),[24a] and 1-(*N*-methylamino)pent-4-ene (**11**)[24b] were synthesized according to literature procedures. 1-(Amino-*N*,*N*-d_2)pent-4-ene (**1d$_2$**), 2-(amino-*N*,*N*-d_2)hex-5-ene (**5d$_2$**), and 2,2-dimethyl-1-(amino-*N*,*N*-d_2)pent-4-ene (**9d$_2$**) were synthesized by repeated deuterium exchange with D_2O under N_2 and were found to be ≥98% ND_2 by ^{1}H NMR integration. 1-Aminopent-4-ene (**1**),[12a,e] 1-aminohex-5-ene (**3**),[12a,h] 2-methyl-1-aminopent-4-ene (**7**),[12a] and *o*-allylaniline (**13**)[25] were synthesized via modifications of literature methods as described. Substrates **1**, **3**, **5**, **7**, **9**, **11**, and **15** were

(6) For leading reviews on intermolecular hydroamination, see: (a) Brunet, J. J.; Neibecker, D.; Neidercorn, F. *J. Mol. Catal.* **1989**, *49*, 235–259. (b) Gasc, M. B.; Lattes, A.; Perie, J. J. *Tetrahedron* **1983**, *39*, 703–731. (c) Trost, B. M.; Verhoeven, T. R. *Comprehensive Organometallic Chemistry*; Wilkinson, G.; Stone, F. G. A.; Abel, E. W., Eds.; Pergamon Press: Oxford, 1982.

(7) (a) Schaad, D. R.; Landis, C. R. *J. Am. Chem. Soc.* **1990**, *112*, 1628–1629. (b) Casalnuovo, A. L.; Calabrese, J. C.; Milstein, D. *J. Am. Chem. Soc.* **1988**, *110*, 6738–6744. (c) Cowan, R. L.; Trogler, W. C. *Organometallics* **1987**, *6*, 2451–2453.

(8) (a) Pez, G. P.; Galle, J. E. *Pure Appl. Chem.* **1985**, *57*, 1917–1926. (b) Clerici, M. G.; Maspero, F. *Synthesis* **1980**, 305–306.

(9) For an amine-based, zirconocene cation-catalyzed process for functionalizing β-substituted picolines, see: Guran, A. S.; Jordan, R. F.; Taylor, D. F. *J. Am. Chem. Soc.* **1991**, *113*, 1833–1835.

(10) (a) For the addition of NH_3 to $H_2C{=}CH_2$, $\Delta G° \approx -4$ kcal mol^{-1}.[10b] (b) Pedley, J. B.; Naylor, R. D.; Kirby, S. P. *Thermochemical Data of Organic Compounds*, 2nd ed.; Chapman and Hall: London, 1986; Appendix Table 1.2.

(11) *Kirk-Othmer Encyclopedia of Chemical Technology*, 3rd ed.; John Wiley & Sons: New York, 1978; Vol. 1, pp 272–278; Vol. 2, pp 740–751.

(12) (a) Tamaru, Y.; Hojo, M.; Higashima, H.; Yoshida, Z. *J. Am. Chem. Soc.* **1988**, *110*, 3994–4002 and references therein. These authors summarize the strengths and weaknesses of group 10-catalyzed hydroamination. (b) Reference 1c, Chapters 7.4, 17.1. (c) Hegedus, L. S.; Akermark, B.; Zetterberg, K.; Olsson, L. F. *J. Am. Chem. Soc.* **1984**, *106*, 7122–7126. (d) Hegedus, L. S.; McKearin, J. M. *J. Am. Chem. Soc.* **1982**, *104*, 2444–2451 and references therein. (e) Pugin, B.; Venanzi, L. M. *J. Organomet. Chem.* **1981**, *214*, 125–133 and references therein. (f) Lathbury, D.; Vernon, P.; Gallagher, T. *Tetrahedron Lett.* **1986**, *27*, 6009–6012.

(13) (a) Deeba, M.; Ford, M. E. *J. Org. Chem.* **1988**, *53*, 4594–4596. (b) Deeba, M.; Ford, M. E.; Johnson, T. A. *J. Chem. Soc., Chem. Commun.* **1987**, 562–563.

(14) A catalytic hydroamination of alkynes has recently been reported to occur via a zirconocene imido complex ($Cp_2Zr{=}NR$): Baranger, A. M.; Walsh, P. J.; Bergman, R. G. *Abstracts of Papers*, 199th National Meeting of the American Chemical Society, Boston, MA, April 1990; American Chemical Society: Washington, DC, 1990; INOR 594.

(15) (a) Mauermann, H.; Marks, T. J. *Organometallics* **1985**, *4*, 200–202. (b) Jeske, G.; Lauke, H.; Mauermann, H.; Swepston, P. N.; Schumann, H.; Marks, T. J. *J. Am. Chem. Soc.* **1985**, *107*, 8091–8103. (c) Jeske, G.; Schock, L. E.; Mauermann, H.; Swepston, P. N.; Schumann, H.; Marks, T. J. *J. Am. Chem. Soc.* **1985**, *107*, 8103–8110. (d) Jeske, G.; Lauke, H.; Mauermann, H.; Schumann, H.; Marks, T. J. *J. Amer. Chem. Soc.* **1985**, *107*, 8111–8118. (e) Watson, P. L.; Parshall, G. W. *Acc. Chem. Res.* **1985**, *18*, 51–55.

(16) General organolanthanide references: (a) Schumann, H. In *Fundamental and Technological Aspects of Organo-f-Element Chemistry*; Marks, T. J., Fragala, I., Eds.; D. Reidel: Dordrecht, The Netherlands, 1985; Chapter 1. (b) Evans, W. J. *Adv. Organomet. Chem.* **1985**, *24*, 131–177. (c) Kagan, H. B.; Namy, J. L. In *Handbook on the Physics and Chemistry of Rare Earths*; Gschneider, K. A., Eyring, L., Eds.; Elvesier: Amsterdam, 1984; Chapter 50. (d) Marks, T. J.; Ernst, R. D. *Comprehensive Organometallic Chemistry*; Wilkinson, G., Stone, F. G. A., Abel, E. W., Eds.; Pergamon Press: Oxford, 1982; Chapter 21.

(17) Stoichiometric insertion of nitriles and alkynes into metal–nitrogen bonds has recently been observed for organoscandium and -zirconium hydrazido complexes: (a) Shapiro, P. J.; Henling, L. M.; Marsh, R. E.; Bercaw, J. E. *Inorg. Chem.* **1990**, *29*, 4560–4565. (b) Walsh, P. J.; Hollander, F. J.; Bergman, R. G. *J. Am. Chem. Soc.* **1990**, *112*, 894–896.

(18) Cp'_2LaNMe_2 catalyzes ethylene polymerization (Hedden, D.; Marks, T. J. Unpublished results).

(19) (a) Nolan, S. P.; Stern, D.; Hedden, D.; Marks, T. J. *ACS Symp. Ser.* **1990**, *428*, 159–174. (b) Nolan, S. P.; Stern, D.; Marks, T. J. *J. Am. Chem. Soc.* **1989**, *111*, 7844–7853.

(20) $\Delta H_{calcd} \approx -5$ to 0 kcal mol^{-1} for eq 4 using existing Th,[20a] Zr,[20b] Sm,[19] and other Ln[19] data. (a) Bruno, J. W.; Marks, T. J.; Morss, L. R. *J. Am. Chem. Soc.* **1983**, *105*, 6824–6832. (b) Schock, L. E.; Marks, T. J. *J. Am. Chem. Soc.* **1988**, *110*, 7701–7715.

(21) Fagan, P. J.; Manriquez, J. M.; Vollmer, C. H.; Day, C. S.; Day, V. M.; Marks, T. J. *J. Am. Chem. Soc.* **1981**, *103*, 2206–2220.

(22) (a) Gagné, M. R.; Marks, T. J. *J. Am. Chem. Soc.* **1989**, *111*, 4108–4109. (b) Gagné, M. R.; Marks, T. J. *Abstracts of Papers*, 197th National Meeting of the American Chemical Society, Dallas, TX, April 9–14; American Chemical Society: Washington, DC, 1989; INOR 32.

(23) Fendrick, C. M.; Schertz, L. D.; Mintz, E. A.; Marks, T. J. *Inorg. Synth.*, in press.

(24) (a) Harding, K. E.; Burks, S. R. *J. Org. Chem.* **1981**, *46*, 3920–3922. (b) Perie, J. J.; Laval, J. P.; Roussel, J.; Lattes, A. *Tetrahedron* **1972**, *28*, 675–699.

(25) (a) Hurd, C. D.; Jenkins, W. W. *J. Org. Chem.* **1957**, *22*, 1418–1423. (b) Smith, P. A. S.; Chou, S. S. P. *J. Org. Chem.* **1981**, *46*, 3970–3977.

predried over KOH, freeze–thaw degassed, and vacuum-distilled from Na/K alloy. The amino olefin **13** was dried by repeated additions to freshly activated 4-Å molecular sieves and degassed by freeze–pump–thaw methods. The complexes $(Cp'_2LaH)_2$,[15b] $Cp'_2LaCH(TMS)_2$,[15b] $Cp'_2NdCH(TMS)_2$,[15b] $Cp'_2LaN(TMS)_2$,[26a] $Cp'_2NdN(TMS)_2$,[26b] $Cp'_2SmCH(TMS)_2$,[15b] $Cp'_2LuCH(TMS)_2$,[15b] $Cp'_2YCH(TMS)_2$,[27] $Me_2SiCp''_2NdCH(TMS)_2$ ($Cp'' = \eta^5$-Me_4C_5),[15c] $Me_2SiCp''_2SmCH(TMS)_2$,[15c] $Me_2SiCp''_2LuCH(TMS)_2$,[15c] $Me_2SiCp''_2YCH(TMS)_2$,[15c] $Et_2SiCpCp''LuCH(TMS)_2$,[28] and $Et_2SiCpCp''YCH(TMS)_2$[28] were synthesized according to published procedures.

1-Aminopent-4-ene (1). The following procedure was found to be more amenable to scale-up than previously described methods.[12a,e] Bromopent-4-ene, 75 g (0.50 mol), was heated at 60 °C for 24 h with 102 g (0.55 mol) of potassium phthalimide in 1 L of DMF. After cooling to room temperature, the solution was filtered, added to 1 L of 50:50 saturated NaCl/H_2O, and extracted three times with ether (1000 mL total). The ether extracts were washed with a saturated NaCl solution (100 mL) and dried over K_2CO_3. The ether solution was then filtered and the solvent removed from the filtrate by rotary evaporation to give *N*-pent-4-enylphthalimide.[29] This material was used without further purification. *N*-pent-4-enylphthalimide and 25 g (0.50 mol) of hydrazine monohydrate were heated overnight at 60 °C in 600 mL of EtOH. After the solution was cooled to room temperature, concentrated HCl (175 mL) was added dropwise and the solution refluxed for an additional 2 h. After cooling, the solution was filtered and a white precipitate collected by filtration and washed with additional EtOH (200 mL). The filtrate was concentrated by rotary evaporation and the residual EtOH removed in vacuo at 60 °C overnight. The amine was isolated by adding 400 mL of H_2O, made alkaline with KOH pellets, and extracted three times with diethyl ether (1000 mL total). The ether phase was washed with a saturated NaCl solution, dried over Na_2SO_4, and filtered. The solvent was next removed by rotary evaporation at room temperature, followed by prolonged (2 h) rotary evaporation at 0 °C to yield a pale yellow oil, which was dried over KOH and distilled (bp 124 °C) to yield 21.0 g of **1** (0.247 mol, 49% yield). The *O*-tosylate of 4-penten-1-ol may also be substituted for bromopent-4-ene. The ^{1}H NMR (400 MHz, $CDCl_3$) data agree with literature data:[12a,e] δ 5.8 (m, 1 H, C*H*=CH_2), 5.0 (m, 2 H, CH=CH_2), 2.71 (t, J = 7 Hz, 2 H, H_2NCH_2), 2.12 (q, J = 7.2 Hz, 2 H, CH_2CH=CH_2), 1.54 (m, 2 H, $CH_2CH_2CH_2$), 1.21 (br, 2 H, NH_2).

1-Aminohex-5-ene (3). Compound **3** (0.10 mol, 40% yield) was prepared in an analogous manner to **1** using bromohex-5-ene (40.8 g, 0.25 mol). The ^{1}H NMR (400 MHz, $CDCl_3$) data agree with reported literature spectra:[12a,h] δ 5.8 (m, 1 H, C*H*=CH_2), 5.03 (m, 2 H, CH=CH_2), 2.48 (t, J = 6.6 Hz, 2 H, H_2NCH_2), 1.96 (q, J = 6.8 Hz, 2 H, CH_2CH=CH_2), 1.28 (m, 4 H, $CH_2CH_2CH_2CH$), 0.6 (br, 2 H, NH_2).

2-Methyl-1-aminopent-4-ene (7). This preparation is a modification of the procedure described in ref 12a. Propionitrile, 20 mL (0.28 mol), was added dropwise to a solution of 0.28 mol of lithium diisopropyl amide in 400 mL of THF/175 mL of hexane at −78 °C, and the solution was allowed to stir for 2 h. Allyl bromide, 24 mL (0.28 mol), was added, and the mixture stirred for 2 h at −78 °C and then allowed to warm to room temperature. The solution was next washed with H_2O and 2 N HCl until the extracts were acidic and then washed with a saturated NaCl solution. The organic layer was next dried over Na_2SO_4, filtered, and the solvent removed via rotary evaporation. The monoalkylated nitrile was isolated by fractional distillation to give 4.9 g (0.052 mol, 19% yield) of material (bp 85 °C/100 mm). The amine was obtained via $LiAlH_4$ reduction using the method of Tamaru[12a] to give 3.2 g (0.032 mol, 62% yield) of **7** (bp 59 °C/70 mm, lit.[12e] bp 115–116 °C). The ^{1}H NMR (400 MHz, $CDCl_3$) data agree with published results:[12e] δ 5.80 (m, 1 H, C*H*=CH_2), 5.03 (m, 2 H, CH=CH_2), 2.67 (dd, J = 12.6, 5.9 Hz, H_2NCHH'), 2.52 (dd, J = 12.6, 6.8 Hz, 1 H, H_2NCHH'), 2.16 (m, 1 H, C*H*H'CH=CH_2), 1.92 (m, 1 H, CHH'CH=CH_2), 1.57 (m, 1 H, $CHCH_3$), 1.05 (br, 2 H, NH_2), 0.92 (d, J = 6.7 Hz, 3 H, CH_3).

***o*-Allylaniline (13).** The following is a modified procedure based on ref 25. Under inert atmosphere, 25 g (0.19 mol) of *N*-allylaniline and 25 mL of BF_3/Et_2O were refluxed in 1500 mL of xylenes. After 24 h, an additional 15 mL of BF_3/Et_2O was added and reflux continued. This addition was repeated twice over the next 48 h. The reaction solution was then poured into 1.5 L of 5 N NaOH, the mixture shaken, and the organic layer separated. The organic layer was further extracted three times with 2 N HCl (500 mL total). The acidic aqueous fraction was then made alkaline with NaOH pellets and extracted with Et_2O (1000 mL total). The ether solution was washed with a saturated NaCl solution, dried over Na_2SO_4, filtered, and the solvent removed by rotary evaporation. The amine was recrystallized as the hydrochloride salt from absolute EtOH. The ^{1}H NMR (400 MHz, $CDCl_3$) data agreed with published spectra:[25b] δ 7.05 (m, 2 H), 6.75 (t, J = 7.6 Hz, 1 H), 6.68 (d, J = 8 Hz, 1 H), 5.95 (m, 1 H, C*H*=CH_2), 5.10 (m, 2 H, CH=CH_2), 3.66 (br, 2 H, NH_2), 3.30 (d, J = 6 Hz, 2 H, CH_2CH=CH_2).

2,2-Dimethyl-1-aminohept-6-ene (15). This new amino olefin was synthesized in a two-step procedure from isobutyronitrile (4.62 g, 67 mmol) and bromopent-5-ene (10.00 g, 67 mmol) using the general method described in ref 12a. The nitrile precursor to **19** was obtained in 82% yield (7.56 g, 55 mmol) and was purified by vacuum distillation (70 °C/1 mm): ^{1}H NMR (400 MHz, $CDCl_3$) δ 5.84 (m, 1 H, C*H*=CH_2), 5.05 (m, 2 H, CH=CH_2), 2.14 (dt, J = 6.8, 6.9 Hz, 2 H, CH_2CH=CH_2), 1.55–1.65 (m, 4 H, $CH_2CH_2CH_2CH$=CH_2), 1.49 (s, 6 H, $(CH_3)_2$); ^{13}C NMR (100 MHz, $CDCl_3$) δ 138.2 (*C*H=CH_2), 125.5 (*C*≡N), 115.6 (CH=*C*H_2), 41.0 ($CH_2C(CH_3)_2$), 34.1 (CH_2CH_2CH=CH_2), 32.8 ($C(CH_3)_2$), 27.3 ($C(CH_3)_2$), 25.1 (CH_2CH=CH_2); MS (rel abundance) $M^+ - 1$ (1.8), 122 (8), 109 (26), 94 (26), 81 (13), 69 (78), 54 (36), 41 (100); IR (Nujol, cm^{-1}) $\nu_{C\equiv N}$ 2275 (vs), $\nu_{C=C}$ 1645 (s), $\nu_{=CH}$ 3120 (m). Anal. Calcd for $C_9H_{15}N$: C, 78.78; H, 11.12; N, 10.21. Found: C, 78.59; H, 11.25; N, 9.98. The nitrile (7.10 g, 36.7 mmol) was reduced[12a] to give amine **15** in 71% purified yield, (bp 61 °C/1 mm): ^{1}H NMR (400 MHz, $CDCl_3$) δ 5.84 (m, 1 H, C*H*=CH_2), 5.00 (m, 2 H, CH=CH_2), 2.47 (s, 2 H, CH_2NH_2), 2.07 (dt, J = 7, 7.3 Hz, 2 H, CH_2CH=CH_2), 1.37 (m, 2 H, CH_2), 1.22 (m, 2 H, CH_2), 0.98 (br, 2 H, NH_2), 0.88 (s, 6 H, $C(CH_3)_2$); ^{13}C NMR (100 MHz, $CDCl_3$) δ 138.3 (*C*H=CH_2), 113.9 (CH=*C*H_2), 52.5 (NH_2CH_2), 38.6 ($C(CH_3)_2CH_2$-CH_2), 34.4 (CH_2CH_2CH=CH_2), 34.1 ($C(CH_3)_2$), 24.4 ($C(CH_3)_2$), 23.1 (CH_2CH=CH_2); MS (rel abundance) M^+ (1), $M^+ - 1$ (1), $M^+ + 1$ (1), 126 (14), 98 (9), 84 (8), 69 (100), 55 (76), 41 (95); IR (Nujol, cm^{-1}) ν_{NH} 3430 (w), 3350 (w), $\nu_{=CH}$ 3120 (m), $\nu_{C=C}$ 1645 (s). Anal. Calcd for $C_9H_{19}N$: C, 76.06; H, 13.47; N, 9.86. Found: C, 76.10; H, 13.79; N, 9.74.

2,6,6-Trimethylhomopiperidine (16). This cyclized amine was synthesized as described in the typical NMR-scale reactions using $Me_2SiCp''_2NdCH(TMS)_2$ as the precatalyst: ^{1}H NMR (400 MHz, C_6D_6) δ 2.52 (m, 1 H, C*H*CH_3), 2.41 (d, J = 14 Hz, C*H*H'NH), 2.28 (d, J = 13.6 Hz, CH*H'*NH), 1.46–1.63 (m, 2 H, CH_2), 1.28–1.38 (m, 2 H, CH_2), 1.12–1.20 (m, 2 H, CH_2), 1.02 (s, 3 H, $C(CH_3)(CH_3')$), 0.91 (d, J = 6.4 Hz, 3 H, $CHCH_3$), 0.80 (s, 3 H, $C(CH_3)(CH_3')$), 0.77 (br, 1 H, N*H*); ^{13}C NMR (100 MHz, C_6D_6) δ 60.7 (*C*H_2NH), 57.2 (*C*H-CH_3NH), 42.2 (CH_2), 41.0 (CH_2), 35.3 ($C(CH_3)_2$), 29.5 ($C(CH_3)(CH_3')$), 28.1 ($C(CH_3)(CH_3')$), 24.1 ($CHCH_3$), 22.1 (CH_2); MS (rel abundance) M^+ (38), $M^+ - 1$ (5), $M^+ + 1$ (16), 126 (83), 98 (86), 84 (42), 70 (43), 58 (100).

$Cp'_2LaNHC_2H_5(H_2NC_2H_5)$ (17). Into a solution of 254 mg (0.447 mmol) of $Cp'_2LaCH(TMS)_2$ in 20 mL of pentane at −78 °C was condensed a 10-fold excess of ethylamine (dried over Na). Upon mixing, the yellow solution immediately became colorless. Under an argon atmosphere, the solution was allowed to slowly warm to ambient temperature and stirred an additional hour. The solvent was then removed under vacuum, and the white solids were dried under high vacuum for 30 min. Next, 10 mL of pentane was vacuum-transferred into the flask at −78 °C, the resulting mixture was warmed and stirred for 15 min, the pentane was removed in vacuo, and the residue was dried in vacuo for 30 min. This procedure was repeated twice to remove any $CH_2(TMS)_2$ byproduct. Next, 10 mL of pentane was condensed into the flask, the flask was warmed to room temperature, and the clear colorless solution was filtered. The filtrate was then slowly cooled to −40 °C and cold-filtered to yield 145 mg (0.291 mmol, 65% yield) of colorless crystalline **17**: ^{1}H NMR (400 MHz, toluene-d_8, 45 °C) δ 2.90 (br, 4 H, CH_2), 1.98 (s, 30 H, Cp'), 1.48 (br, 3 H, N*H*), 0.98 (t, 6 H, CH_3); ^{1}H NMR (400 MHz, toluene-d_8, −77 °C) δ 3.61 (br m, 2 H, J = 6.8 Hz, $NHCH_2$), 2.92 (t, J = 8.5 Hz, 1 H, N*H*), 2.20 (m, 2 H, NH_2CH_2), 2.09 (s, 30 H, Cp'), 1.31 (t, J = 6.4 Hz, 3 H, CH_3), 0.75 (t, J = 6.8 Hz, 3 H, CH_3), 0.45 (br, 2 H, NH_2); ^{13}C NMR (100 MHz, toluene-d_8, 80 °C) δ 116.7 (C_5Me_5), 41.3 (CH_2CH_3), 21.5 (CH_2CH_3), 11.1 (C_5Me_5); ^{13}C NMR (100 MHz, toluene-d_8, −89 °C) δ 115.9 (CCH_3, Cp'), 45.3 ($NHCH_2$), 37.9 (H_2NCH_2), 24.7 ($NHCH_2CH_3$), 17.9 ($H_2NCH_2CH_3$), 11.6 (CH_3, Cp');[30] ^{13}C CPMAS (75 MHz, 5-mm rotor, 3800-Hz spinning speed) δ

(26) (a) $Cp'_2LaN(TMS)_2$ was synthesized using the method described in ref 26b. (b) Tilley, T. D.; Andersen, R. A. *Inorg. Chem.* **1981**, *20*, 3267–3270.

(27) den Haan, K. H.; deBoer, J. L.; Teuben, J. H.; Spek, A. L.; Kojić-Prodić, B.; Hays, G. R.; Huis, R. *Organometallics* **1986**, *5*, 1726–1733.

(28) (a) Stern, D.; Sabat, M.; Marks, T. J. *J. Am. Chem. Soc.* **1990**, *112*, 9558–9575. The $SiEt_2$ bridge imparts significantly enhanced solubility over the $SiMe_2$ analogues. (b) Stern, D. Ph.D. Thesis, Northwestern University, Evanston, IL, 1990.

(29) Maruyama, K.; Ogawa, T.; Kubo, Y.; Araki, T. *J. Chem. Soc., Perkin Trans. 1* **1985**, 2025–2031.

(30) (a) These assignments are tentatively based on the ^{13}C NMR chemical shifts of the free amines, which for $CH_3CH_2NH_2$ and CH_3NH_2 are δ 17.7, 35.9 ppm and 26.9 ppm, respectively.[30b] (b) Silverstein, R. M.; Bassler, G. C.; Morrill, T. C. *Spectrometric Identification of Organic Compounds*, 4th ed.; Wiley: New York, 1981; pp 227–236.

116.7, 115.3 (C_5Me_5), 45.0 (NH_2CH_2), 37.3 (br, $NHCH_2$), 23.7 (CH_3), 15.9 (CH_3), 12.0, 11.4 (C_5Me_5); IR (Nujol, cm^{-1}) ν_{NH} 3356 (sh, w), ν_{NH} 3332 (w), ν_{NH} 3280 (m). Anal. Calcd for $C_{24}H_{43}N_2La$: C, 57.82; H, 8.69; N, 5.62; MW, 499. Found: C, 57.94; H, 8.46; N, 5.39; MW, 466 ± 54 (cryoscopy in benzene). Alternatively, $Cp'_2LaN(TMS)_2$ can be used as the starting material with no adverse effects on yield.

$Cp'_2LaNHCH_3(H_2NCH_3)$ (18). This complex was synthesized analogously to **17** using 260 mg of $Cp'_2LaN(TMS)_2$ (0.457 mmol) and a 5-fold excess of CH_3NH_2 (dried over Na) in 15 mL of pentane at −78 °C. This solution was stirred for 10 min and then warmed to ambient temperature under Ar. After stirring at room temperature, the clear solution was filtered, concentrated, and slowly cooled to −78 °C to induce crystallization. Cold filtration and drying in vacuo afforded 110 mg (0.26 mmol, 57% yield) of colorless, crystalline **18**: ^1H NMR (400 MHz, toluene-d_8, 53 °C) δ 2.57 (6 H, NCH_3), 1.94 (30 H, Cp′), 1.28 (3 H, NH); ^1H NMR (400 MHz, toluene-d_8, −98 °C) δ 3.52 (d, J = 6.4 Hz, 3 H, CH_3), 2.99 (br, 1 H, NH), 2.09 (30 H, Cp′), 1.74 (s, 3 H, CH_3), −0.06 (br, 2 H, NH_2); ^{13}C NMR (100 MHz, toluene-d_8, 50 °C) δ 116.5 (C_5Me_5), 11.2 (C_5Me_5); ^{13}C NMR (100 MHz, toluene-d_8, −100 °C) δ 115.9 (C_5Me_5), 37.5 ($NHCH_3$), 29.4 (H_2NCH_3), 11.5 ($C_5(CH_3)$;[30] ^{13}C CPMAS (75 MHz, 5-mm rotor, 10 300-Hz spinning speed) δ 115.8 (br, C_5Me_5), 38.0 ($NHCH_3$), 29.0 (NH_2CH_3), 11.4, 10.9 (C_5Me_5); IR (Nujol, cm^{-1}) ν_{NH} 3371 (w), 3322 (w), 3280 (w), and 3162 (w). Anal. Calcd for $C_{22}H_{39}N_2La$: C, 56.17; H, 8.35; N, 5.95; MW, 470. Found: C, 56.18; H, 8.64; N, 5.87; MW, 447 ± 33 (cryoscopy in benzene).

$Cp'_2NdNHC_2H_5(H_2NC_2H_5)$ (19). This complex was prepared in a manner similar to **17** using 423 mg (0.738 mmol) of $Cp'_2NdCH(TMS)_2$. By slow cooling the resulting filtered solution, 290 mg (0.577 mmol, 78% yield) of blue crystalline **19** was obtained: ^1H NMR (400 MHz, C_6D_6, 25 °C) δ 5.04 (30 H, Cp′, $\Delta\nu_{1/2}$ = 8.6 Hz), no amine resonances are observed at ambient temperature; IR (Nujol, cm^{-1}) ν_{NH} 3350 (sh, w), 3288 (w), 3342 (m). Anal. Calcd for $C_{24}H_{43}N_2Nd$: C, 57.21; H, 8.60; N, 5.56. Found: C, 57.37; H, 8.67; N, 5.43.

$Cp'_2La\overline{NCH_2C(CH_3)_2CH_2CHCH_3}(H\overline{NCH_2C(CH_3)_2CH_2CHCH_3})$ (20). Into a solution of 260 mg (0.458 mmol) of $Cp'_2LaCH(TMS)_2$ in 10 mL of pentane at −78 °C was vacuum-transferred 0.460 mmol of **9** (28 Torr in a 300-mL volume). The pale yellow solution immediately turned colorless upon mixing. The mixture was allowed to warm slowly to room temperature with stirring under argon. After the mixture stirred for 1 h at ambient temperature, the solvent was removed under vacuum. The resulting colorless oil was triturated three times with 10 mL of pentane, yielding a colorless solid. Pentane (10 mL) was vacuum-transferred into the flask, warmed to room temperature, and the resulting solution filtered under argon. The pale yellow solution was slowly cooled to −78 °C and allowed to stand overnight. The solution was cold-filtered and the colorless crystalline product was collected and dried under vacuum (150 mg, 0.236 mmol, 52% yield). Interestingly, at low temperatures pentane solutions of **20** are colorless but at ambient temperatures they are pale yellow: IR (Nujol, cm^{-1}) ν_{NH} 3295 (w); ^1H NMR (400 MHz, toluene-d_8, 0 °C) δ 4.40 (m, 1 H), 3.40 (d, 1 H), 3.16 (m, 1 H), 2.80 (d, 1 H), 2.57 (dd, 1 H), 2.48 (t, 1 H), 2.09 (s, 30 H), 1.98 (m, 1 H), 1.75 (dd, 1 H), 1.47 (dd, 1 H), 1.29 (d, 3 H), 1.28 (s, 3 H), 1.07 (s, 3 H), 1.05 (d, 3 H), 0.89 (s, 3 H), 0.84 (s, 3 H); ^{13}C NMR (100 MHz, toluene-d_8, 0 °C) δ 117.9 (CCH_3, Cp′), 62.5 (t, J_{CH} = 133 Hz, CH_2), 61.0 (t, J_{CH} = 133 Hz, CH_2), 58.8 (d, J_{CH} = 132 Hz, CH), 55.9 (d, J_{CH} = 138 Hz, CH), 52.9 (t, J_{CH} = 125 Hz, CH_2), 48.6 (t, J_{CH} = 129 Hz, CH_2), 40.8 (s, CMe_2), 39.8 (s, CMe_2), 29.8 (q, J_{CH} = 124 Hz, CH_3), 29.2 (q, J_{CH} = 123 Hz, CH_3), 28.2 (q, J_{CH} = 123 Hz, CH_3), 27.1 (q, J_{CH} = 123 Hz, CH_3), 26.2 (q, J_{CH} = 122 Hz, CH_3), 23.4 (q, J_{CH} = 126 Hz, CH_3), 14.4 (q, J_{CH} = 124 Hz, CCH_3, Cp′). Anal. Calcd for $C_{34}H_{59}N_2La$: C, 64.34; H, 9.37; N, 4.41; MW, 635. Found: C, 64.13/64.31; H, 9.16/9.20; N, 3.98/3.95; MW, 591 ± 81 (by cryoscopy in benzene).

$Cp'_2La\overline{N(CH_2)_3CHCH_3}(H\overline{N(CH_2)_3CHCH_3})$ (21) was prepared in an analogous manner to **20** using 205 mg (0.361 mmol) of $Cp'_2LaCH(TMS)_2$ and (25 Torr) 300 mL of **1** in 20 mL of pentane at −78 °C. After the mixture was stirred under argon for 18 h at ambient temperature, the solvent was removed in vacuo, followed by two successive triturations with 10 mL of pentane. White crystalline **21** was obtained by slow-cooling a pentane solution (95 mg, 0.16 mmol, 44% yield): ^1H NMR (400 MHz, toluene-d_8, 0 °C) δ 4.35 (m, 1 H), 3.45 (q, 1 H), 2.99 (m, 2 H), 2.62 (m, 1 H), 2.43 (m, 1 H), 2.06 (s, 30 H), 1.75–1.9 (m, 2 H), 1.4–1.6 (m, 4 H), 1.15 (d, 3 H), 0.92 (m, 1 H), 0.88 (d, 3 H); ^1H NMR (400 MHz, toluene-d_8, −77 °C) δ 2.17, 2.16, 2.12, 2.09 (s, Cp′); ^{13}C NMR (100 MHz, toluene-d_8, 0 °C) δ 117.8 (CCH_3, Cp′), 57.7 (d, J_{CH} = 131 Hz, CH), 55.2 (d, J_{CH} = 140 Hz, CH), 47.4 (t, J_{CH} = 135 Hz, 2 C, CH_2), 35.2 (t, J_{CH} = 125 Hz, CH_2), 33.8 (t, J_{CH} = 131 Hz, CH_2), 26.6 (t, J_{CH} = 128 Hz, CH_2), 26.2 (t, J_{CH} = 130 Hz, CH_2), 24.5 (q, J_{CH} = 123 Hz, CH_3), 21.9 (q, J_{CH} = 128 Hz, CH_3), 11.7 (q, J_{CH} = 124 Hz, CCH_3, Cp′); ^{13}C NMR (100 MHz, toluene-d_8, −77 °C) δ 117.7, 117.4, 117.2, 117.0, and 116.8 (CCH_3, Cp′), 58.2, 58.1, 55.2, and 54.8 (CH), 48.2, 47.8, 47.3, and 46.9 (CH_2), 35.2, 35.1, 33.8, and 33.5 (CH_2), 27.0 (t, J_{CH} = 131 Hz, CH_2), 26.9 (t, J_{CH} = 128 Hz, CH_2), 26.5 (t, J_{CH} = 130 Hz, CH_2), 26.4 (t, J_{CH} = 125 Hz, CH_2), 24.7, 24.6, 22.4, and 21.8 (CH_3), 12.3 (q, J_{CH} = 123.6 Hz), 12.2 (q, J_{CH} = 123.6 Hz), 12.0 (q, J_{CH} = 123.7 Hz), 11.9 (q, J_{CH} = 123.7 Hz, CCH_3, Cp′); IR (Nujol, cm^{-1}) ν_{NH} 3308 (w). Anal. Calcd for $C_{30}H_{51}N_2La$: C, 62.27; H, 8.88; N, 4.84; MW, 579. Found: C, 62.53/62.39; H, 9.17/8.92; N, 4.50/4.53; MW, 546 ± 54 (by cryoscopy in benzene).

In Situ Characterization of $Cp'_2LaNHCH_2CMe_2CH_2CH{=}CH_2$-($H_2NCH_2CMe_2CH_2CH{=}CH_2$). Into a 5-mm NMR tube equipped with a resealable Teflon valve were charged 11.2 mg (19.7 μmol) of $Cp'_2LaCH(TMS)_2$ and 800 μL of toluene-d_8. On a high-vacuum line, the sample was degassed by evacuation at −78 °C, and 2 equiv of **9** was vacuum-transferred from a calibrated gas bulb. Under an argon atmosphere, the solution was mixed at −78 °C and then inserted into the precooled probe of the VXR-400 spectrometer: ^1H NMR (400 MHz, toluene-d_8, −60 °C) δ 6.02 (m, 1 H, $CH{=}CH_2$), 5.59 (m, 1 H, $CH{=}CH_2$), 5.20 (m, 2 H, $CH{=}CH_2$), 5.04 (m, 2 H, $CH{=}CH_2$), 3.27 (d, J = 8.8 Hz, 2 H, $CH_2CH{=}CH_2$), 2.83 (t, J = 8.4 Hz, 1 H, LaNH), 2.29 (t, J = 8.5 Hz, 2 H, NCH_2CMe_2), 2.08 (s, 30 H, C_5Me_5), 1.61 (d, J = 7.3 Hz, 2 H, $CH_2CH{=}CH_2$), 1.14 (m, 2 H), 1.02 (s, 6 H, CMe_2), 0.57 (s, 6 H, CMe_2), the NH_2 resonance was not located.

Typical NMR-Scale Catalytic Reaction. In the glove box, the $Cp'_2LaCH(TMS)_2$ precatalyst (ca. 10 mg, 18 μmol) was loaded into an NMR tube equipped with a Teflon valve. On the high-vacuum line, the tube was evacuated and 700 μL of toluene-d_8 was vacuum-transferred into the tube, followed by 2-aminohex-5-ene (**5**) (0.64 mmol, 36-fold molar excess) from a calibrated volume gas bulb. The tube was then sealed and the reaction monitored by ^1H NMR.

Isotopic Labeling Studies. $2d_2$. The deuterated cyclized amine was synthesized as described in the above section using 10 mg of $Cp'_2LaCH(TMS)_2$ (18 μmol) and 100 mg of **$1d_2$** (1.15 mmol, 64-fold excess) in C_6D_6. The reported spectrum and H–D coupling constants are consistent with the ^1H NMR spectrum described in ref 12e for **$2d_1$**: ^1H NMR (400 MHz, toluene-d_8) δ 2.85 (m, 2 H), 2.60 (m, 1 H), 1.60 (m, 1 H), 1.50 (m, 2 H), 0.93–1.03 (m, 1 H), 1.00 (dt, J_{HH} = 6.4 Hz, J_{HD} = 2 Hz, 2 H, CH_2D);[12e] ^{13}C NMR (100 MHz, C_6D_6) δ 54.5 (d, J_{CH} = 134 Hz, $CHCH_2D$), 47.0 (t, J_{CH} = 136 Hz, CH_2ND), 34.0 (t, J_{CH} = 129 Hz, CH_2CHCH_2D), 26.1 (t, J_{CH} = 129 Hz, CH_2CH_2ND), 21.3 (ttd, J_{CH} = 124 Hz, J_{CD} = 19 Hz, $^2J_{CH}$ = 7 Hz, $CHCH_2D$).

***cis*-$6d_2$.** The amine was synthesized in an analogous manner to **$2d_2$** using **$5d_2$**: ^1H NMR (400 MHz, toluene-d_8) δ 2.90 (m, 1 H, CHND), 1.67 (m, 2 H, CHH′), 1.15 (m, 2 H, CHH′), 1.05 (d, 3 H, J = 6.0 Hz, CH_3), 1.03 (dt, 2 H, J_{HH} = 6.4 Hz, J_{HD} = 2.0 Hz, CH_2D); ^{13}C NMR (400 MHz, ^1H-decoupled, toluene-d_8) δ 54.83 ($CHCH_3$), 54.76 (s, $CHCH_2D$), 33.95 (s, CH_2CHCH_3), 33.92 (s, CH_2CHCH_2D), 22.06 (s, CH_3), 21.77 (t, J_{CD} = 19 Hz, CH_2D); ^{13}C NMR (400 MHz, ^1H-coupled, toluene-d_8) δ 54.74 (d, J_{CH} = 138 Hz, CHND), 33.91 (t, J_{CH} = 128 Hz, CH_2CHND), 22.06 (q, J_{CH} = 124 Hz, CH_3), 21.78 (tt, J_{CH} = 121 Hz, J_{CD} = 20 Hz, CH_2D).

***trans*-$6d_2$.** The amine was synthesized in an analogous manner to **$2d_2$** using **$5d_2$**: ^1H NMR (400 MHz, toluene-d_8) δ 3.13 (m, 1 H, CHNH), 1.77 (m, 2 H, CHH′), 1.08 (m, 2 H, CHH′), 0.99 (d, 3 H, J = 6.4 Hz, CH_3), 0.97 (dt, 2 H, J_{HH} = 6.4 Hz, J_{HD} = 2.0 Hz, CH_2D); ^{13}C NMR (400 MHz, ^1H-decoupled, toluene-d_8) δ 53.37 ($CHCH_3$), 53.31 (s, $CHCH_2D$), 35.18 (s, CH_2CHCH_3), 35.14 (s, CH_2CHCH_2D), 22.65 (s, CH_3), 22.35 (t, J_{CD} = 19 Hz, CH_2D); ^{13}C NMR (400 MHz, ^1H-coupled, toluene-d_8) δ 53.35 (d, J_{CH} = 140 Hz, CHND), 35.18 (t, J_{CH} = 128 Hz, CH_2CHND), 22.66 (q, J_{CH} = 124 Hz, CH_3), 22.34 (tt, J_{CH} = 125 Hz, J_{CD} = 20 Hz, CH_2D).

$10d_2$. The amine was synthesized in an analogous manner to **$2d_2$** using **$9d_2$**: ^1H NMR (400 MHz, toluene-d_8) δ 3.05 (m, 1 H), 2.62 (d, J = 10.1 Hz, 1 H), 2.46 (d, J = 9.9 Hz, 1 H), 1.48 (dd, J = 12.2, 6.9 Hz, 1 H), 0.95 (m, 1 H), 1.03 (dt, J_{HH} = 6.2 Hz, J_{HD} = 1.9 Hz, CH_2D); ^{13}C NMR (100 MHz, toluene-d_8) δ 62.22 (t, J_{CH} = 137 Hz, CH_2ND), 55.21 (d, J_{CH} = 131 Hz, CHND), 50.85 (t, J_{CH} = 126 Hz, CH_2CHCH_3), 40.54 (s, $C(CH_3)_2$), 30.09 (q, J_{CH} = 124 Hz, $C(CH_3)CH_3$), 29.08 (q, J_{CH} = 124 Hz, $C(CH_3)CH_3$), 22.96 (ttd, J_{CH} = 122 Hz, J_{CD} = 19 Hz, $^2J_{CH}$ = 6 Hz, $CHCH_2D$).

Preparative-Scale Catalytic Reactions. In the glove box, 43 mg (76 μmol) of $Cp'_2LaCH(TMS)_2$ was loaded into a 15-mL round-bottom reaction flask equipped with a magnetic stir bar. At −78 °C, 2 mL of pentane was vacuum-transferred onto the catalyst followed by 2.2 mL of **1** (1.69 g, 19.9 mmol). The clear, colorless solution was stirred under argon for 24 h at ambient temperature. The reaction mixture was then freeze–thaw degassed and the volatiles were vacuum-transferred into a separate flask. Pentane was removed on the rotary evaporator at 0 °C to give 1.45 g (12.8 mmol, 86% yield, >95% pure by GC/MS) of **2**.

Alternatively for nonvolatile products such as **14**, filtration through silica gel effectively removes the catalyst.

Kinetic Studies of Hydroamination/Cyclization. In a typical experiment, an NMR sample was prepared as described above (see the Typical NMR-Scale Catalytic Reaction section) but maintained at −78 °C until kinetic measurements were begun. The sample tube was then inserted into the probe of the XL-400 spectrometer which had been previously set to the appropriate temperature ($T \pm 0.2$ °C, checked with a methanol or ethylene glycol temperature standard). A long pulse delay was used during data acquisition to avoid saturation. The kinetics were usually monitored from intensity changes in the substrate olefinic resonances over 3 or more half-lives.

The substrate concentration C was measured from the olefin peak area, A_s, standardized to the area, A_l, of free $CH_2(TMS)_2$ in solution ($C = A_s/A_l$). The $CH_2(TMS)_2$ arises via quantitative ligand elimination during catalyst generation (Scheme I). All data could be convincingly fit by least-squares to eq 6, where C_0 is the initial concentration of substrate ($C_0 = A_{s0}/A_{l0}$). The ratio of catalyst to substrate (E) was accurately determined from the ratio of A_{s0} and A_{l0}. The turnover frequency (h^{-1}) was calculated from the least-squares-determined x intercept ($-C_0/m$, min) according to eq 7.

$$C = mt + C_0 \tag{6}$$

$$N_t\ (h^{-1}) = (60\ \text{min}\ h^{-1}/(-C_0/m))E \tag{7}$$

Diastereoselectivity Study of (*R*,*S*)-5 Cyclization. All cyclization survey reactions were carried out in standard 5-mm NMR tubes equipped with Teflon valves. Typical reaction concentrations involved 10 mg of lanthanide alkyl (~18 μmol) and a 7–150-fold molar excess of **5**. Reactions were run at ambient temperature and monitored by ^1H NMR. Upon completion, the volatiles were vacuum-transferred and subsequently analyzed by ^1H NMR for isomer ratio.

In the case where the isomer ratio was monitored over the extent of conversion, the ^1H NMR experiment was conducted as described above in the Typical NMR-Scale Reaction section. The sample solution was inserted into the probe of the XL-400 at 25.0 ± 0.2 °C, and the reaction was monitored using a pulse delay of at least 10 s to avoid saturation. The trans:cis ratio was determined using integration techniques on the α-CH resonance of the trans at δ 3.15 and the cis multiplet at 2.94 ppm.[24a] Kinetic analyses were similar to those described above.

Diastereoselectivity Study of (*R*,*S*)-5 Cyclization in the Presence of *n*-Propylamine. As described above, 10 mg (0.018 mmol) of $Cp'_2LaCH(TMS)_2$ was loaded into a 5-mm NMR tube equipped with a Teflon valve. The tube was evacuated on the high-vacuum line, and 700 μL of toluene-d_8 was vacuum-transferred at −78 °C. Sequentially, 0.31 mmol of (*R*,*S*)-**5** and 0.80 mmol of *n*-propylamine were vacuum-transferred from calibrated volume glass bulbs. After 5 h at ambient temperature, NMR analysis showed the reaction to be 56% complete, and after an additional 12 h, >98% complete. Vacuum transfer of the volatiles followed by NMR analysis showed the ratio of *trans*-**6**:*cis*-**6** to be ≥50:1.

Competitive Inhibition Kinetics. These measurements were carried out using the XL-400 spectrometer. In the glove box, 57.4 mg of $Cp'_2LaCH(TMS)_2$ (0.10 mmol) was dissolved in 5.0 mL of toluene-d_8 to make a 20.1 mM solution. Into each of several standard 5-mm NMR tubes containing resealable Teflon valves was loaded a 600-μL aliquot of this solution. On the high-vacuum line, the appropriate quantities of **9** and *n*-propylamine were vacuum-transferred from calibrated gas bulbs into the tubes kept at −78 °C. Quick warming and insertion into the NMR probe that had been previously equilibrated to 25.0 ± 0.2 °C initiated the experiment. Data were acquired using four scans with a minimum pulse delay of 10 s. Absolute concentrations of **9** and *n*-propylamine were obtained by integrating the olefinic resonance of **9** (δ 4.95) and the CH_2 multiplet of *n*-propylamine (δ 1.26) and comparing them to the TMS resonance of $CH_2(TMS)_2$ at δ 0.02. Velocity data (M s^{-1}) were obtained by integration of third-order polynomial fits to [substrate] (M) versus time (s) plots and used for subsequent 1/velocity vs 1/[substrate] and velocity vs [inhibitor]/[substrate] plots. The generated velocity vs [I]/[S] plots were numerically fit to eq 29 using the nonlinear least-squares analysis feature of the Kaleidograph software package.

X-ray Crystallographic Study of $Cp'_2LaNHCH_3(H_2NCH_3)$ (18). Large, colorless crystals of **18** were grown by slow-cooling a concentrated pentane solution to −25 °C. Single crystals were isolated from the mother liquor by direct addition of suitably dried and degassed Paratone N (Exxon) to the cold solution. The pentane was decanted, and suitable single crystals were located in the oil, mounted on a glass fiber, and transferred directly to the −120 °C cold stream of an Enraf-Nonius CAD4 diffractometer. Subsequent computations were carried out on a microVax 3600 computer.

Table I. Summary of the Crystal Structure Data for $Cp'_2LaNHCH_3(H_2NCH_3)$ (**18**)

formula	$2(La_1C_{24}H_{43}N_2)$
cryst syst	monoclinic
space group	$P2_1/n$
a, Å	19.901 (4)
b, Å	11.695 (3)
c, Å	20.202 (3)
β, deg	97.95 (2)
V, Å^3	4656 (2)
Z	4
d_{calcd}, g/cm^3	1.342
cryst size, mm	0.1 × 0.4 × 0.5
color, habit	yellow, transparent
diffractometer	Enraf-Nonius, CAD4
temp	−120 °C
μ, cm^{-1}	18.48
transmission factors range	0.799–0.506 (numerical)
radiation	graphite monochromator; Mo Kα, λ = 0.71069
scan type	ω/θ
2θ range, deg	2–48 ($+h,-k,\pm l$)
intensities (unique, R_i)	8077 (7291, 0.066)
intensities > $2.58\sigma(I)$	3296
no. of params	452
R	0.049
R_w for $w = 1/\sigma^2(F_o) + \rho F_o^2$	0.063 (ρ = 0.030)
max density in ΔF map, e/Å^3	1.25

Crystal data collection parameters are listed in Table I. Lattice parameters were determined from 25 high-angle reflections, and cell reduction calculations showed **18** to crystallize in the monoclinic space group $P2_1/n$ (No. 14).[31] Intensities of 3 standard reflections were measured every 1.5 h of X-ray exposure and showed no significant variations. Intensity data were corrected for Lorentz, polarization, and anomalous dispersion effects.[32] A numerical absorption correction was also applied with minimum and maximum transmission factors of 0.506 and 0.799, respectively. The structure was solved using Patterson methods (SHELXS-86).[33a] Full-matrix least-squares refinement (SHELX-76)[33b] with anisotropic thermal parameters for all nonhydrogen atoms gave a final $R(F)$ of 0.049 and $R_w(F)$ = 0.063. Hydrogen atoms attached to carbon atoms were given "idealized" positions and treated as fixed contributors with a common isotropic thermal parameter. Hydrogen atoms on nitrogen did not surface on the difference Fourier map and were not included in the structure factors. The largest peak in the final difference map (1.25 e Å^{-3}) was located near the lanthanum center.

Results

This section begins with comments on alternative routes into the catalytic manifold of the present system, followed by an examination of the broad reaction scope in terms of product ring size and regio- and diastereoselectivity of heterocycle formation. Variations of catalyst turnover frequency with π-ancillary ligation and metal ion size are then discussed. A kinetic study of the hydroamination/cyclization reaction includes in situ examination of molecularity, activation parameters, ND/NH kinetic isotope effects, solvent dependences, and competitive inhibition by unreactive substrate analogues. To model components of the proposed cycle, the complex $Cp'_2LaNHCH_3(H_2NCH_3)$ (**18**) was synthesized and the molecular structure characterized both in solution and in the solid state. Also discussed are in situ variable-temperature ^1H NMR experiments of active catalytic solutions.

Catalyst Generation. Several routes into the catalytic manifold of Scheme I have been developed from Cp'_2LnR (R = H, η^3-C_3H_5, $CH(TMS)_2$, $N(TMS)_2$; Ln = La, Nd, Sm, Y, Lu) precursors. For these complexes, rapid and quantitative proton transfer (within seconds as monitored by ^1H NMR) occurs from the substrate to the ligand R, generating HR and the catalytically active lanthanide

(31) Cromer, D. T.; Waber, J. T. *International Tables for X-ray Crystallography*; The Kynoch Press: Birmingham, England, 1974; Vol. IV, pp 175–181.

(32) Reference 31, Vol. IV, pp 149–150.

(33) (a) Sheldrick, G. M. In *Crystallographic Computing*; Sheldrick, G. M., Kruger, C., Goddard, R., Eds.; Oxford University Press: Oxford, 1985; pp 175–189. (b) Sheldrick, G. M. SHELX-76, A Program for Crystal Structure Determination, University Chemical Laboratory, Cambridge, England, 1976.

Table II. Catalytic Results for the Organolanthanide-Catalyzed Hydroamination/Cyclization of Amino Olefins[a]

entry	substrate	product	N_t, h^{-1} (°C)
1	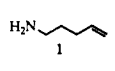 1	 2	140 (60)[b]
2	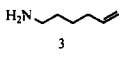 3	 4	5 (60)[b]
3	 5	 6	45 (25)[b]
4	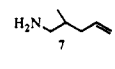 7	 8	36 (25)[b]
5	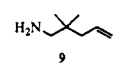 9	 10	95 (25)[b]
6	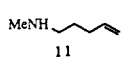 11	 12	11 (25)[c]
7	 13	 14	12 (80)[b]
8	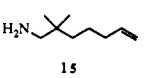 15	 16	0.3 (60)[c]

[a] All rates measured in toluene-d_8. [b] Rate measured using $Cp'_2LaCH(TMS)_2$ as the precatalyst. [c] Rate measured using $Me_2SiCp''_2NdCH(TMS)_2$ as the precatalyst.

amido species. The mechanism of protonolysis likely involves amine precoordination followed by a well-documented rapid four-centered protonolysis transition state (A,[34] eq 8), forming the active catalytic species and eliminating alkane. Literature

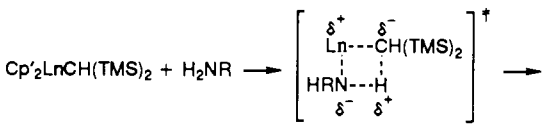

A

$$Cp'_2LnNHR + CH_2(TMS)_2 \quad (8)$$

precedent for base coordination in sterically congested $Cp'_2LnCH(TMS)_2$ environments is provided by the coordination of $^tBuC{\equiv}N$ to $Cp'_2CeCH(TMS)_2$.[35] Of particular relevance to simplified catalyst synthesis is the ligand R = $N(TMS)_2$, derived from $KN(TMS)_2$, which serves as an inexpensive, commercially available reagent for the preparation of halide- and base-free catalyst precursors.[26] Kinetic studies show the catalytic activity for the cyclization **1** → **2** (Table II) to be independent of the precursor R group examined, suggesting a common active intermediate. Generation of the active species with the bulky substrate **9** ($t_{1/2}$ for consumption of $Cp'_2LaN(TMS)_2 \approx 60$ min) is much slower than with **1**, leading to a brief induction period. $Cp'_2LnN(TMS)_2$ complexes therefore provide a straightforward entry into the catalytic manifold shown in Scheme I.

Hydroamination catalyst generation from readily prepared[36] divalent $Cp'_2Sm(THF)_2$ was recently reported[37] and is proposed

Scheme I

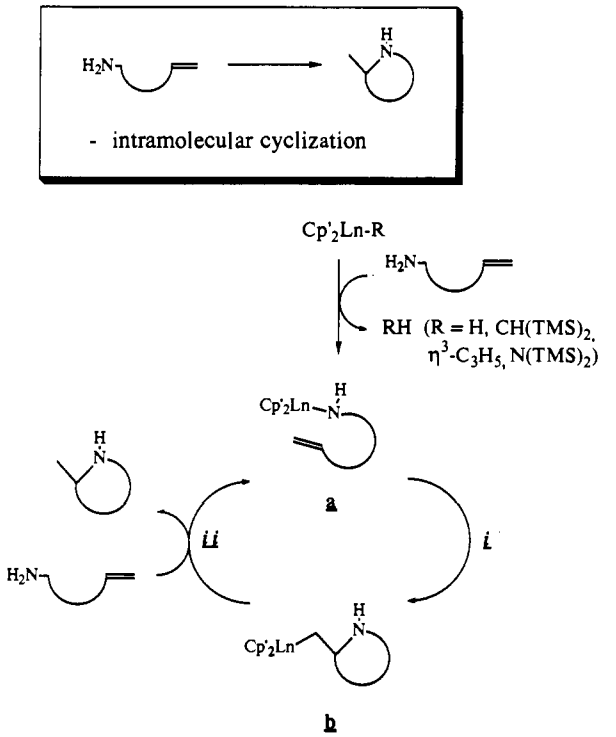

to occur via binuclear oxidative allylic CH activation. This process generates Cp'_2SmH and $Cp'_2Sm(\eta^3\text{-allyl})$ (eq 9), both of which undergo reaction with primary and secondary amines to afford catalytically active $Cp'_2SmNR'R$ complexes. The $Cp'_2Sm(THF)_2$

$$2Cp'_2Sm + CH_2{=}CHCH_2R \rightarrow Cp'_2SmH + Cp'_2Sm(\eta^3\text{-allyl}) \quad (9)$$

and $Cp'_2LnN(TMS)_2$ catalyst precursors thus have the advantage of being easier and more economical to synthesize than hydride or $CH(TMS)_2$ complexes. Details of the interesting oxidative behavior of Sm(II) complexes in the presence of amino olefins are deferred to a later contribution.

Hydroamination/Cyclization Scope. In an effort to probe the scope of this catalytic hydroamination/cyclization reaction, various survey substrates were examined with respect to chemo- and regioselectivity, substituent effects, and turnover frequency. The results are shown in Table II. It can be seen that the present process is effective in the catalytic formation of five-, six-, and even seven-membered heterocycles. The transformation of **11** → **12** (Table II) illustrates that organolanthanide-catalyzed cyclizations are not restricted to primary amines and that secondary amines also undergo cyclization using $Me_2SiCp''_2NdCH(TMS)_2$ (25 °C, Cp'' = η^5-Me_4C_5) and $Cp'_2SmCH(TMS)_2$ (60 °C)[37a] as precatalysts.[38] This cyclization methodology is also applicable to aromatic amino olefins as exemplified by the synthesis of 2-methylindoline (**13** → **14**). Thus, as shown in Table II, organolanthanide-catalyzed olefin hydroamination/cyclization is effective for primary (entries 1–5, 7, 8), secondary (entry 6), and aromatic amino olefins (entry 7), as well as amines having nitrogen at primary (entries 1, 2, 4, 5, 8), secondary (entry 3), and aromatic (entry 7) carbon positions.

When using $4f^n$ catalysts ($n \neq 0$ or 14) such as $Cp'_2NdCH(TMS)_2$ and $Cp'_2SmCH(TMS)_2$, distinct color changes occur concurrently with catalytic initiation and termination. Thus, the green and orange solutions of the neodymium and samarium alkyl precatalysts immediately turn to the characteristic blue and yellow colors of the respective amine complexes[37a] upon substrate (amine) addition (even at −78 °C). Upon consumption of the excess

(34) (a) Piers, W. E.; Shapiro, P. J.; Bunel, E. E.; Bercaw, J. E. *Synlett* **1990**, 74–84. (b) Doherty, N. M.; Bercaw, J. E. *J. Am. Chem. Soc.* **1985**, *107*, 2670–2682. (c) Thompson, M. E.; Baxter, S. M.; Bulls, A. R.; Burger, B. J.; Nolan, M. C.; Santarsiero, B. D.; Schaefer, W. P.; Bercaw, J. E. *J. Am. Chem. Soc.* **1987**, *109*, 203–219.

(35) Heeres, H. J.; Renkema, J.; Booij, M.; Meetsma, A.; Teuben, J. H. *Organometallics* **1988**, *7*, 2495–2502.

(36) Evans, W. J.; Grate, J. W.; Chei, H. W.; Bloom, I.; Hunter, W. E.; Atwood, J. L. *J. Am. Chem. Soc.* **1985**, *107*, 941–946.

(37) (a) Gagné, M. R.; Nolan, S. P.; Marks, T. J. *Organometallics* **1990**, *9*, 1716–1718. (b) Catalytic rate depression is only observed at high THF concentrations. When 1–2 equiv of THF are present, cyclization rates are indistinguishable from THF-free reaction solutions.

(38) The $Cp'_2LaCH(TMS)_2$-catalyzed reaction affords low product yields (~10%) due to a catalyst deactivation process. The nature of the process as well as the identity of the deactivated catalyst is currently under investigation.

Table III. Metal, Temperature, and Ancillary Ligand Effects on the *trans*:*cis*-2,5-Dimethylpyrrolidine (6) Ratio Arising from the Cyclization of 2-Aminohex-5-ene ((*R*,*S*)-**5**)[a]

lanthanide		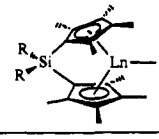	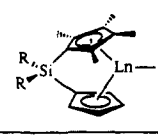
La	8:1 (0 °C) 5:1 (25 °C) 3:2 (50 °C) ≥50:1 (25 °C)[b] 2:1 (25 °C)[c]		
Nd	1:1.25 (25 °C) 4:1 (25 °C)[b]	20:1 (25 °C)	
Sm	1:1.25 (25 °C)	1:1 (25 °C)	
Y	8:1 (25 °C)	3:1 (25 °C)	18:1 (25 °C)
Lu			4:1 (25 °C)

[a] All reactions carried out with similar catalyst to substrate ratios and in toluene-d_8 unless otherwise indicated. [b] Reaction carried out in the presence of 3 molar equiv of *n*-propylamine, based on starting substrate concentration. [c] Reaction carried out in neat THF-d_8.

Table IV. Metal Size Effects on the Turnover Frequencies for **9** → **10** in Toluene-d_8

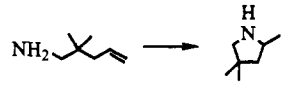

catalyst	ionic radius, Å	N_t, h^{-1} (°C)
Cp'_2La-	1.106	95 (25)
Cp'_2Sm-	1.079	48 (60)
Cp'_2Lu-	0.977	<1 (80)

substrate, the reaction solutions return to their original colors. General workup conditions for preparative-scale reactions involve vacuum transfer of the volatiles from the catalyst, or with non-transferable substrates, filtration through a short column of silica gel followed by solvent removal. In all cases, the products are isolated in >85% yield and are >95% pure by GC/MS. ^{1}H NMR spectra of completed in situ monitored experiments show only resonances attributable to cyclized product, with no traces of starting material or other heterocyclic regioisomers. All reactions are found to proceed equally well in pentane, toluene, benzene, and related hydrocarbon solvents. In donor solvents such as THF, catalytic rates are significantly slower (for **9** → **10**, N_t (initial) = 18 h^{-1} in THF at 25 °C, $k_{toluene}/k_{THF}$ = 5.3 (5)).[37b,39]

The cyclization of **5** → **6** (eq 10) affords mixtures of *trans*- and *cis*-2,5-dimethylpyrrolidine (B, C). The B:C isomer ratio is highly dependent on lanthanide ion size, π-ligation, reaction temperatures, and added exogenous ligands. Table III shows the isomer ratios

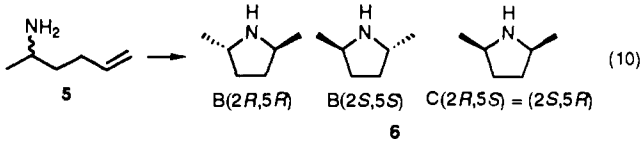

(10)

for a variety of lanthanide and ligand environments. In general, lower temperatures afford higher trans:cis ratios. A systematic variation of the degree of congestion in the coordination environment shows maximum trans:cis ratios of 20:1 and 18:1 using the $Me_2SiCp''_2YCH(TMS)_2$ and $Et_2SiCpCp''LuCH(TMS)_2$ precatalysts, respectively. Higher or lower coordinative unsaturation gives lower ratios.[40] *trans*-**6** is a useful C_2 chiral directing agent,[41,42] and the straightforward synthesis described here is an

(39) The catalytic consequences of competition for vacant Cp'_2LnR coordination site(s) by Lewis bases has been noted previously.[15]

(40) Typical Pd^{2+} and Pt^{2+} catalysts give a 60:40 trans/cis mixture for 6 and a 40:60 mixture for **8**.[12e]

(41) For a review of the use of C_2 ligands in organic synthesis, see: Whitesell, J. K. *Chem. Rev.* **1989**, *89*, 1581–1590.

Table V. π-Ancillary Ligation Effects on the Turnover Frequencies for **9** → **10** in Toluene-d_8

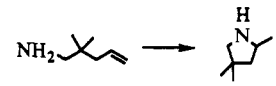

catalyst	N_t, h^{-1} (°C)
Cp'_2Lu-	<1 (80)
$R_2SiCp''_2Lu$-	75 (80)
$R_2SiCpCp''Lu$-	200 (80)

example of the potential utility of the present catalytic system. In interesting contrast to **6**, the diastereomeric product ratios in the **7** → **8** transformation (Table II, eq 11) are insensitive to the steric environment, giving consistently 1:1 to 1:1.5 ratios of trans:cis isomers, D:E.[40] Remarkably, it is also observed that the addition

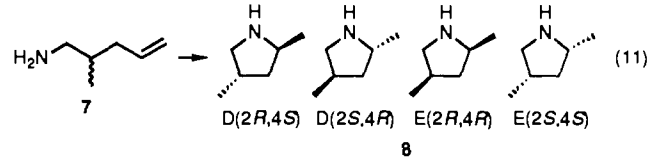

(11)

of a noncyclizable substrate analogue such as *n*-propylamine drastically alters the diastereoselectivity of reaction **5** → **6** (Table III). When the cyclization catalyzed by $Cp'_2LaCH(TMS)_2$ is carried out in the presence of a 3-fold molar excess of *n*-propylamine, an increase in the trans:cis product ratio from 5:1 to ≥50:1 is observed. Kinetically, the reaction exhibits a depressed turnover frequency due to competitive inhibition by *n*-propylamine (vide infra). Additionally, the $Cp'_2NdCH(TMS)_2$-catalyzed **5** → **6** transformation exhibits an increase in the trans:cis product ratio from 1:1.25 to 3.8:1 under identical conditions (Table III).

Metal and Ancillary Ligation Effects on the Hydroamination/Cyclization Process. Preliminary kinetic studies of the $Cp'_2LaCH(TMS)_2$-catalyzed hydroamination/cyclization process suggested that the turnover-limiting step is olefin insertion/cyclization (i in Scheme I). Since such a sterically sensitive step should reflect subtle changes in the catalyst coordination environment, a study of the turnover frequency as a function of metal ionic radius and ancillary ligation was undertaken. For the

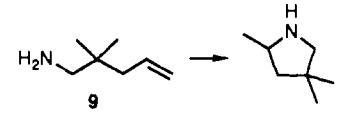

(12)

cyclization of **9** → **10** (eq 12), Table IV shows that the variation in N_t proceeding from the lanthanide with the largest eight-coordinate ionic radius, La[43] (1.160 Å), to intermediate, Sm (1.079 Å), and to smallest, Lu (0.977 Å), spans over 3 orders of magnitude. Similar to the aforementioned Cp'_2La system, the Sm catalyst also shows zero-order kinetics in the substrates for over 3 half-lives.

The effect of the supporting π-ligation on the hydroamination/cyclization rates was also probed for **9** → **10** (eq 12), and the rates obtained for catalysts with modified ligand environments are set out in Table V. All reactions were zero-order in substrate for the reaction times monitored (usually 2 or more half-lives). For the sterically demanding Cp'_2Lu environment, low catalytic activity is observed. Replacement of this environment with $Me_2SiCp''_2$ ligation[44] dramatically increases the rate to 75

(42) Examples of the synthetic utility of *trans*-6 are given in the following: (a) Porter, N. A.; Scott, D. M.; Rosenstein, I. J.; Giese, B.; Veit, A.; Zeitz, H. G. *J. Am. Chem. Soc.* **1991**, *113*, 1791–1799. (b) Geise, B.; Zehnder, M.; Roth, M.; Zietz, H. *J. Am. Chem. Soc.* **1990**, *112*, 6741–6742. (c) Schlessinger, R. H.; Iwanowicz, E. J.; Springer, J. P. *J. Org. Chem.* **1986**, *51*, 3070–3073.

(43) (a) Representative eight-coordinate effective ionic radii:[43b] La(III), 1.160 Å; Nd(III), 1.109 Å; Sm(III), 1.079 Å; Y(III), 1.019 Å; Yb(III), 0.985 Å; Lu(III), 0.977 Å. (b) Shannon, R. D. *Acta Crystallogr., Sect. A* **1976**, *A32*, 751–767.

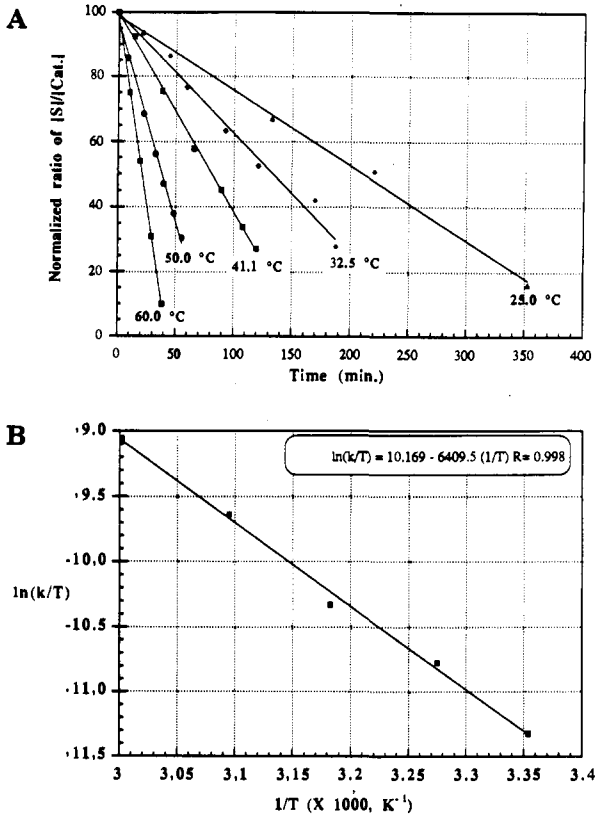

Figure 1. A. Normalized ratio of substrate to lanthanide concentration as a function of time and temperature for the hydroamination/cyclization of $H_2N(CH_2)_3CH{=}CH_2$ (**1**) using the precatalyst $Cp'_2LaCH(TMS)_2$ in toluene-d_8 (see text for details). B. Eyring plot for the hydroamination/cyclization of $H_2N(CH_2)_3CH{=}CH_2$ (**1**) using a $Cp'_2LaCH(TMS)_2$ precatalyst in toluene-d_8. The line is the least-squares fit to the data points.

h^{-1} (80 °C), as does the further modified $Et_2SiCpCp''$[28] ancillary ligand (200 h^{-1} at 80 °C). Another example of ancillary ligand reactivity modulation is in the cyclization of **11** → **12** where Cp'_2La results in no detectable catalysis at 60 °C (18 h, 25-fold excess of substrate), whereas $Me_2SiCp''_2Nd$ (1.109 Å)[43] catalyzes the reaction at 25 °C with N_t = 11 h^{-1}.

Kinetic Studies of Hydroamination/Cyclization. Most of the kinetic data acquired in this study were obtained using the precatalyst $Cp'_2LaCH(TMS)_2$. The rationale for this choice is 2-fold: diamagnetic La^{3+} allows convenient NMR monitoring of reactions, and as previously discussed, the large ionic radius leads to increased cyclization rates (vide supra), thus allowing greater efficiency and accuracy in kinetic measurements on less reactive substrates. The use of $Cp'_2LaCH(TMS)_2$ as a precatalyst also has the advantage of producing $CH_2(TMS)_2$ (δ 0.2 ppm) upon initiation. This byproduct serves as an internal NMR integration standard of appreciable intensity which can be readily distinguished from the substrate, product, and catalyst signals (see the Experimental Section).

In situ ^{1}H NMR studies of all $Cp'_2LaCH(TMS)_2$-catalyzed hydroamination/cyclization reactions indicate that, within detection limits, only the substrate, product, and one lanthanide complex are present in detectable quantities at all degrees of conversion during the reaction. Figure 1 presents kinetic data typical of many runs, which show the rate to be zero-order in substrate to at least 3 half-lives. The hydroamination/cyclization is observed to be zero-order in substrate over at least a 100-fold range (15 mM–1.5 M). Over a 45-fold range in catalyst concentration (1.2–53 mM), the turnover frequency (velocity/[Ln]) is invariant within experimental error, suggesting first-order behavior in catalyst with the rate law, velocity = k_{cycl}[Ln][S]^0. These results coupled with thermodynamic considerations[19,20] (i.e., approximately thermoneutral olefin insertion and exothermic proton transfer) and the documented rapid protonolysis of lanthanide alkyls[21] by amines (eq 5) are consistent with the bulk of the catalyst being present as an amido complex (e.g., a, Scheme I), with olefin insertion being turnover-limiting (i, Scheme I; eq 4). It will be seen in a following section that this amido complex also contains a coordinated amine ligand. Even in the absence of excess amine, the catalyst resting state lies at the amido stage (a, Scheme I) with a coordinated amine as determined by in situ stoichiometric reactions, the products of which are devoid of olefinic ^{1}H NMR features (vide infra). The rate of the **1** → **2** cyclization catalyzed by $Cp'_2LaCH(TMS)_2$ (eq 13) was also monitored by ^{1}H NMR spectroscopy and found to be independent of substrate concentration over a 25–60 °C temperature range. Rate data are shown

Figure 2. Concentration of substrate versus time for the hydroamination/cyclizations of $H_2NCH_2CMe_2CH_2CH{=}CH_2$ (**9**) and $D_2NCH_2CMe_2CH_2CH{=}CH_2$ (**9d$_2$**) using a 20 mM solution of the precatalyst $Cp'_2LaCH(TMS)_2$ in toluene-d_8.

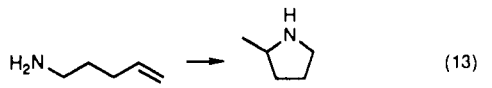

(13)

in Figure 1A normalized to the $CH_2(TMS)_2$ internal standard. Standard Eyring and Arrhenius kinetic analyses[45] (Figure 1B) yield the following activation parameters: $\Delta H^{\ddagger}$ = 12.7 (1.4) kcal mol^{-1}, $\Delta S^{\ddagger}$ = −27.0 (4.6) eu, and E_a = 13.4 (1.5) kcal mol^{-1}.[46]

The products isolated from the cyclization of the deuterated (RND_2) analogues of **1**, **5**, and **9**, **1d$_2$**, **5d$_2$**, and **9d$_2$** respectively, exhibit the deuterium dispositions shown in eqs 14–16. ^{13}C and

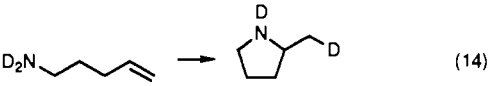

(14)

(15)

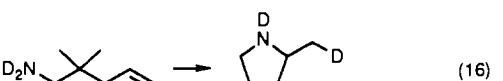

(16)

^{1}H NMR spectra of the cyclized amines show them to be deuterated at the nitrogen and monodeuterated at the 2-methyl

(44) Fendrick, C. M.; Schertz, S. D.; Day, V. M.; Marks, T. J. *Organometallics* **1988**, *7*, 1828–1838.

(45) (a) Robinson, P. J. *J. Chem. Educ.* **1978**, *55*, 509–510. (b) Benson, S. W. *Thermochemical Kinetics*, 2nd ed.; Wiley: New York, 1986; pp 8–10.

(46) Parameters in parentheses represent 3σ values derived from the least-squares fit.

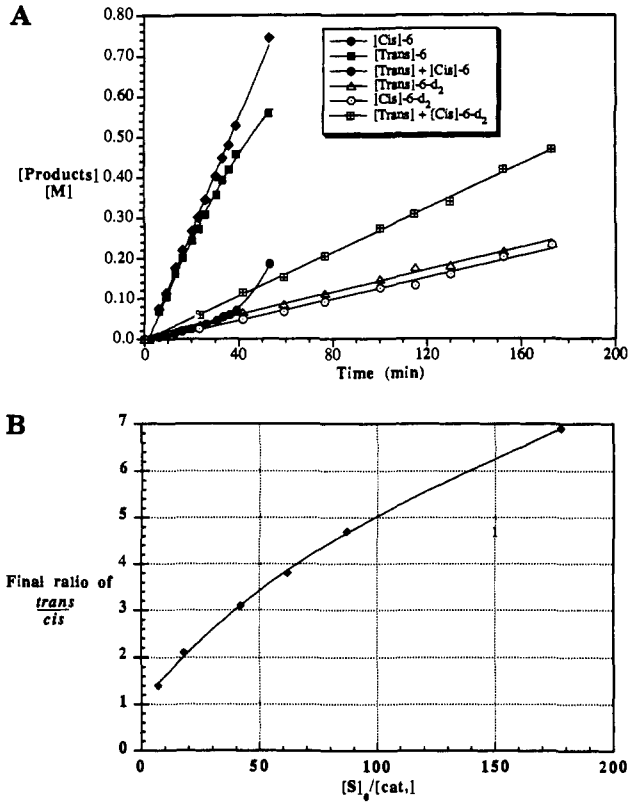

Figure 3. A. Time evolution of the *trans*- and *cis*-2,5-dimethylpyrrolidine (**6**) diastereomers in the cyclization of $H_2NCH(CH_3)(CH_2)_2CH{=}CH_2$ ((*R*,*S*)-**5**) and $D_2NCH(CH_3)(CH_2)_2CH{=}CH_2$ ((*R*,*S*)-**5d$_2$**) using $Cp'_2LaCH(TMS)_2$ as the catalyst precursor in toluene-d_8; [cat.] = 0.020 M, $[(R,S)\text{-}\mathbf{5}]_0$ = 0.84 M, and $[(R,S)\text{-}\mathbf{5d_2}]_0$ = 0.56 M. The lines through the data points are drawn as a guide to the eye. B. Final ratio of trans:cis 2,5-dimethylpyrrolidine (**6**) versus the ratio of initial substrate concentration $[S]_0$ to catalyst concentration [cat.]. In all cases [cat.] = 20 mM. The line through the data points is drawn as a guide to the eye.

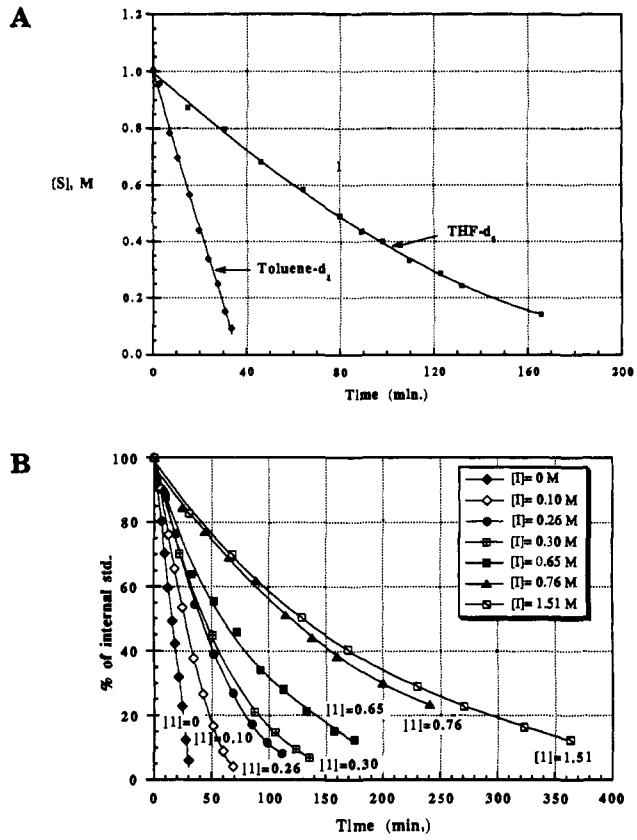

Figure 4. A. Substrate concentration decay curves for the cyclization of $H_2NCH_2CMe_2CH_2CH{=}CH_2$ (**9**) using $Cp'_2LaCH(TMS)_2$ as the catalyst precursor in toluene-d_8 and THF-d_8 at 25.0 °C. Lines through the data points are drawn as a guide to the eye. B. Normalized substrate concentrations for the cyclization of $H_2NCH_2CMe_2CH_2CH{=}CH_2$ (**9**), using $Cp'_2LaCH(TMS)_2$ as the catalyst precursor, as a function of time and concentration of added *n*-propylamine (I); [cat.] = 20 mM in all cases. Lines through the data points are drawn as a guide to the eye, except for [I] = 0, where the line is a least-squares fit.

position to a level ≥95% (see the Experimental Section for details). This regiochemistry is interpreted as resulting from deuterolysis of the intermediate alkyl complex formed upon olefin insertion (ii, Scheme I; eq 5). Additionally, cyclizations with substrates **1d$_2$**, **5d$_2$**, and **9d$_2$** exhibit zero-order kinetics in substrate and rates of 52 h^{-1} (60 °C), 8.8 h^{-1} (25 °C), and 23 h^{-1} (25 °C), respectively, yielding kinetic isotope effects (KIE) of k_H/k_D = 2.7 (4) (60 °C), 5.2 (8) (25 °C), and 4.1 (8) (25 °C), respectively. Figure 2 shows the relative cyclization rates for the diprotio and dideuterio derivatives of **9**, as well as the zero-order dependence on substrate concentration. For **9** and **9d$_2$**, these KIEs are observed to be independent of substrate concentration (0.040–0.22 M in **9d$_2$**; 0.040–1.4 M in **9**), catalyst concentration (2.5–25 mM), and conversion—an important mechanistic observation (vide infra).

Kinetic analysis of the cyclization of racemic **5** ((*R*,*S*)-**5** → **6**) (eq 10) shows typical zero-order kinetics in substrate; however, the ratio of product isomers changes with conversion. Thus, the product mix is initially highly enriched in the trans product, but this excess falls at longer conversion times (Figure 3A). Control experiments with essentially pure *trans*-**6** indicate that the heterocyclic product is not isomerized once formed, while spectropolarimetric analysis of unconverted substrate at various degrees of conversion indicates (as expected) that a kinetic resolution process is not operative, i.e., the substrate remains racemic. That this behavior is a consequence of the substrate concentration at the time of cyclization ([substrate] falls with conversion) is supported by the observation (Figure 3B) that the final *trans*-**6**:*cis*-**6** product ratio obtained is dependent upon the initial substrate:catalyst ratio for constant catalyst concentration. In contrast to **5**, the diastereoselectivity for the cyclization of **5d$_2$** was found to be depressed both in the final levels of *trans*-**6**:*cis*-**6** (~1:1) and with the degree of conversion (Figure 3A). These observations convey important mechanistic implications and interpretation is deferred to the Discussion section.

A depressed cyclization rate for **9** → **10** using $Cp'_2LaCH(TMS)_2$ as the precatalyst is observed in neat THF-d_8,[37b,39] In this case, the kinetics only approach apparent zero-order at high substrate concentrations (Figure 4A). The initial turnover frequency (N_t = 18 h^{-1}, 25 °C) is also lower than in toluene ($k_{toluene}/k_{THF}$ = 5.3 (5)). That the substrate decay curves show a decrease in rate at low amino olefin concentrations suggests that THF acts as a competitive inhibitor under these conditions. From the known tendency of Cp'_2LnR complexes to coordinate Lewis bases (vide infra), a likely inhibition mechanism would invoke THF competition with substrate for the lanthanide coordination site required for olefin insertion.[15] In view of the present substrate, catalyst, and inhibitor concentrations ($[H_2NR] \approx 0.5$ M, [Ln] ≈ 20 mM, [THF] ≈ 12.3 M), the relatively small decrease in rate suggests that at equal concentrations, primary amines are more strongly bound to Cp'_2LaNHR complexes than is THF.[47] Additionally, changes in solvent polarity (stabilization of polar transition state A) may contribute to such a solvent effect. Further remarks about inhibition of the hydroamination/cyclization process are made below.

As in the conversion of **9** → **10** in neat THF-d_8, the cyclization reaction shows significant rate depression upon the addition of measured quantities of the noncyclizable amine, *n*-propylamine. Figure 4B illustrates how the rate of substrate consumption decreases with concentration of added inhibitor (I, *n*-propylamine),

(47) This has also been observed in crystallographically characterized $Cp'_2Yb(NH_3)(THF)$: Wayda, A. L.; Dye, J. L.; Rogers, R. D. *Organometallics* **1984**, *3*, 1605–1610.

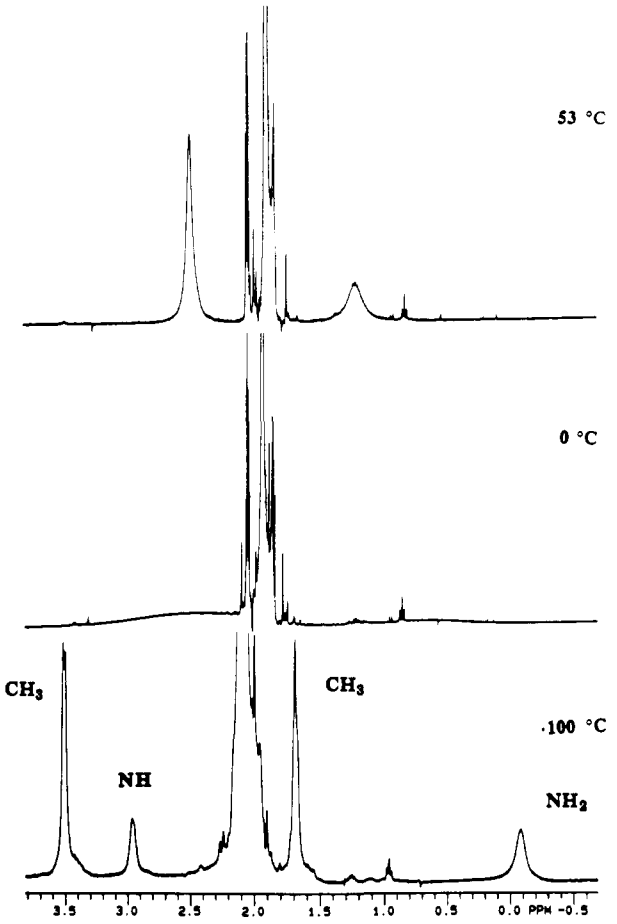

Figure 5. Variable-temperature ^1H NMR spectrum of $Cp'_2LaNHCH_3(H_2NCH_3)$ (**18**) in toluene-d_8 showing the intramolecular proton transfer from coordinated amine to lanthanide amido.

relative to the strictly zero-order behavior observed in its absence ([I] = 0). Kinetic and mechanistic interpretations are deferred to the Discussion section.

Models for Catalytic Species. In an effort to further characterize the individual steps of the catalytic cycle, several model complexes were synthesized. Complexes **17–19** were prepared via metathesis using $Cp'_2LnCH(TMS)_2$ and excess amine (eq 17); see the Experimental Section for characterization data). The

$$Cp'_2LnCH(TMS)_2 + \text{xs } H_2NR \rightarrow Cp'_2LnNHR(H_2NR) + CH_2(TMS)_2 \quad (17)$$

17–19

17: Ln = La, R = Et (65% yield)
18: Ln = La, R = Me (57% yield)
19: Ln = Nd, R = Et (78% yield)

new compounds are soluble in pentane, and upon slow cooling, such solutions afford good yields of colorless and blue crystals of amido complexes[48,49] **17–18** and **19**, respectively. Alternatively, **17** has been synthesized from $Cp'_2LaN(TMS)_2$ by a similar metathetical procedure. The coordinated amine of **17–19** is not removed by recrystallization or by prolonged pumping under dynamic vacuum.

The room temperature ^1H NMR spectrum of **19** shows a single broad resonance at δ 5.04 attributable to a paramagnetically broadened and shifted Cp′ signal,[15a-d] with no amido or amine resonances observable. The ^1H NMR spectrum of diamagnetic **18** is more informative, showing at 53 °C (Figure 5) broad NCH_3 resonances at δ 2.5 and 1.0 ppm, as well as a Cp′ resonance at δ 2.01 (identical in field position to that observed during in situ catalytic experiments). The spectrum is temperature-dependent with the ligand resonances at δ 2.5 and 1.0 ppm continuing to broaden until ca. −22 °C, where individual signals are first resolved. At −100 °C, the limiting spectrum is obtained, which reveals the presence of two inequivalent sets of methyl and NH signals, assignable to methylamido and coordinated methylamine ligands. Spectral integration indicates the presence of one coordinated amine, consistent with the stoichiometry of eq 17. The above spectral changes are reversed upon warming to room temperature and are independent of concentration over a 9-fold range. $\Delta G^{\ddagger}$ for this intramolecular exchange process is 12.0 ± 0.5 kcal mol^{-1} (at 0 °C) using the standard coalescence point formalism.[50] The ethyl derivative behaves similarly, and coalescence point analysis gives $\Delta G^{\ddagger}$ = 12.4 ± 0.5 kcal mol^{-1} (at 0 °C). This dynamic behavior is interpreted in terms of an intramolecular amine-to-amido proton-transfer process, which permutes lanthanide amido and coordinated amine ligands (eq 18). That

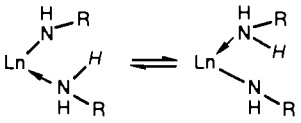

(18)

coalescence of these resonances occurs well below room temperature indicates that under typical catalytic conditions, the lanthanide amido and the bound amine moieties undergo interconversion at rates far in excess of the catalytic turnover frequencies.

The dynamic process observed in the ^1H NMR spectra is also detected in ^{13}C NMR studies of **17**, which at 80 °C show time-averaged APT (attached proton test) resonances for the CH_2 and CH_3 moieties (Figure 6A). However, discrete ethylamine and ethylamido resonances are observed at −77 °C for both sets of CH_2 and CH_3 groups (Figure 6B). At both high (to 80 °C) and low temperatures (to −80 °C), a single set of Cp′ resonances is observed. These observations suggest that either static **17** has mirror symmetry (e.g., F–I, R = Et) or that even at −80 °C an additional dynamic process is permuting instantaneously nonequivalent Cp′ environments (and diastereotopic CH_2 groups) of rotamers in J–L (R = Et). The solution ^1H and ^{13}C NMR spectra

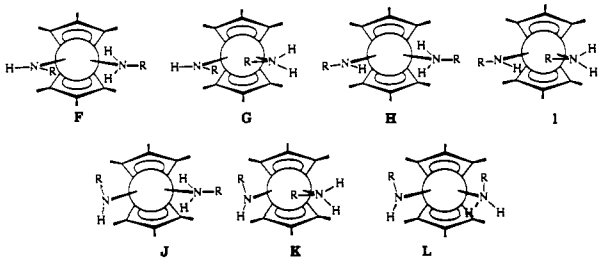

do not distinguish between F–I, which have mirror symmetry, or J–L with rapid rotation about the Ln–N bonds. The solid-state ^{13}C CPMAS spectrum of **17** (Figure 6C) exhibits distinct amine and amido resonances as do the −80 °C solution spectra but, in addition, reveals slightly nonequivalent Cp′ environments (δ 116.7, 117.3; 12.1, 11.4). This result is consistent with the solid-state structure of **18** (vide infra), which has two crystallographically nonequivalent forms of G, each having the N–R vectors rotated out of the N–La–N plane by differing degrees. That is, some multiplicity of nonequivalent Cp′ and *N*-alkyl resonances is an-

(48) Lappert, M.; Power, P. P.; Sanger, A. R.; Srivastava, R. C. *Metal and Metalloid Amides*; Ellis Horwood: Chichester, U.K., 1980.

(49) For examples of other organo–early transition metal, lanthanide, and actinide amido complexes, see: (a) References 21, 26b, and 35. (b) Hillhouse, G. L.; Bercaw, J. E. *J. Am. Chem. Soc.* **1984**, *106*, 5472–5478. (c) Bercaw, J. E.; Davies, D. L.; Wolczanski, P. T. *Organometallics* **1986**, *5*, 443–450 and ref 14 therein. (d) Hillhouse, G. L.; Bulls, A. R.; Santarsiero, B. D.; Bercaw, J. E. *Organometallics* **1988**, *7*, 1309–1312. (e) Hillhouse, G. L.; Bercaw, J. E. *Organometallics* **1982**, *1*, 1025–1029. (f) Mayer, J. W.; Curtis, C. J.; Bercaw, J. E. *J. Am. Chem. Soc.* **1983**, *105*, 2651–2660. (g) Pattiasini, J. W.; Heeres, H. J.; van Bolhuis, F.; Meetsma, A.; Teuben, J. H.; Spek, A. L. *Organometallics* **1987**, *6*, 1004–1010. (h) Hammel, A.; Weidlen, J. *J. Organomet. Chem.* **1990**, *388*, 75–87. (i) Feldman, J.; Calabrese, J. C. *J. Chem. Soc., Chem. Commun.* **1991**, 134–136.

(50) Sandstrom, J. *Dynamic NMR Spectroscopy*; Academic Press: New York, 1982; pp 77–99 and references therein.

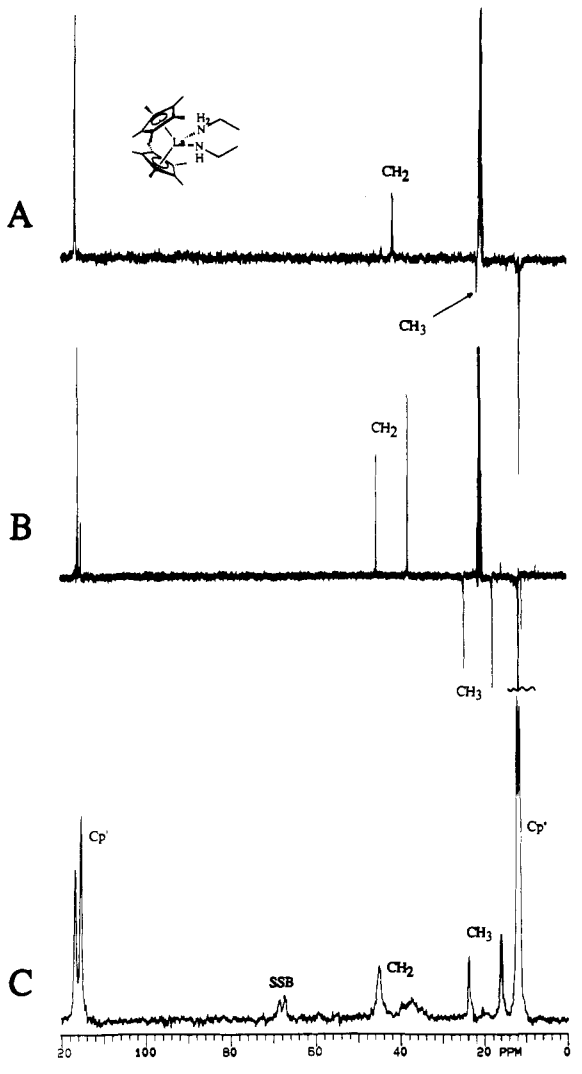

Figure 6. A. Solution ^{13}C NMR APT (attached proton test) spectrum of $Cp'_2LaNHEt(H_2NEt)$ (**17**) at 80 °C demonstrating time-averaged amine and amido environments. B. Solution ^{13}C NMR APT spectrum of $Cp'_2LaNHEt(H_2NEt)$ (**17**) at −100 °C showing the separate resonances for the ethylamine (La←H_2NEt) and ethylamido (La–NHEt) ligands. C. ^{13}C CPMAS of $Cp'_2LaNHEt(H_2NEt)$ (**17**) at ambient temperature showing the existence of two different Me_5C_5 environments. SSB denotes spinning side band.

ticipated. The apparent simplicity of the latter features in the CPMAS spectrum appears to arise from solid-state motional processes and/or, in the case of one or more of the methylene signals, ^{14}N quadrupolar broadening. The infrared spectra of complexes **17–19** exhibit weak ν_{NH} absorptions in the 3200–3400 cm^{-1} region, which are compiled and compared to literature data in Table VI.

There is precedent for Cp'_2MNHR and analogous complexes to coordinate additional Lewis base molecules as well as to undergo interligand proton-exchange processes. The latter are presumed to be *intramolecular* in the amine–amido complexes $Cp'_2CeNH^tBu(H_2N^tBu)$[35] and $Cp'_2ScNHCH_2C_6H_4OMe$-$(NH_2CH_2C_6H_4OMe)$[49c] and have been shown to be *intermolecular* in the exchange reaction of $Cp'_2Hf(H)NH_2$ with $^{15}NH_3$ (to yield $Cp'_2Hf(H)^{15}NH_2$),[49d] Similar concentration-independent proton-transfer processes have been observed in Rh, Ni, Pd, and Pt alkoxide–alcohol complexes.[51] Here an asymmetric hydrogen bridge between the alkoxide and the coordinated alcohol oxygen atom likely mediates the rapid interconversion of alkoxide and alcohol moieties (eq 19).

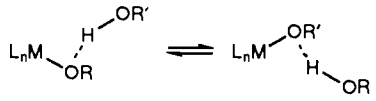

(19)

Table VI. Infrared ν_{NH} Stretching Frequencies (cm^{-1}) for Complexes **17–21** and Selected Literature Comparisons

compd	N–H stretching frequencies, cm^{-1}
$Cp'_2LaNHEt(H_2NEt)$ (**17**)	3356 (w), 3332 (w), 3280 (m)
$Cp'_2LaNHCH_3(H_2NCH_3)$ (**18**)	3371 (w), 3322 (w), 3280 (m), 3162 (w)
$Cp'_2NdNHEt(H_2NEt)$ (**19**)	3350 (sh, w), 3288 (w), 3342 (m)
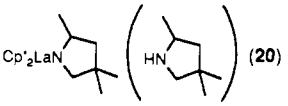 (**20**)	3295 (w)
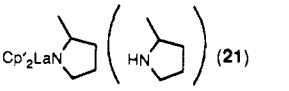 (**21**)	3308 (w)
$Cp'_2ScNHMe$[49c]	3360 (w)
$Cp'_2ScNHCH_2$-*p*-C_6H_4OMe[49c] $(H_2NCH_2$-*p*-$C_6H_4OMe)$	3705 (w), 3360 (m), 3300 (m)
$Cp'_2CeNH^tBu(H_2N^tBu)$[35]	3320 (w), 3260 (w)

Molecular Structure of $(C_5Me_5)_2LaNHCH_3(H_2NCH_3)$ (18). The low-temperature single-crystal X-ray structure determination for **18** indicates the presence of two crystallographically independent monomeric amine–amido complexes in the unit cell (Figure 7). Data collection information, final atomic coordinates,[52a] and relevant bond distances and angles with estimated standard deviations are set out in Tables I, VII, and VIII. The $(Me_5C_5)_2La$ portion of each monomeric unit is unexceptional, with an average C–C ring distance of 1.41 (2, 5, 20) Å,[52] C–CH_3 distance of 1.51 (2, 4, 20) Å, and La–C ring distance of 2.85 (2, 4, 20) Å. The ring-centroid–La–ring-centroid angles of 136.3 (4)° and 140.8 (4)° are similar for both complexes and compare favorably with other early Cp'_2Ln complexes.[15b,35] Interestingly, the N–La–N angle differs slightly between the two molecules, with an angle of 95.4 (3)° for molecule A and 92.4 (3)° for molecule B. These angle differences are additionally manifested in the N–N nonbonded distances of 3.73 (1) and 3.62 (1) Å for molecules A and B, respectively.

Metrical parameters consistent with discrete amine and amido coordination modes are observed in the La–N bond-length disparities of ~0.4 Å.[53] The La–$NHCH_3$ bond lengths of 2.323 (10) and 2.302 (10) Å are observed for molecules A and B, respectively. When compared (after correction for trivalent eight-coordinate ionic radii)[43b] with Ln–N distances in previously characterized lanthanide amido complexes $(Cp'_2YN(TMS)_2$; 2.415 (5) Å calculated, 2.274 (5) Å actual;[54] (*S*)-Me_2Si-$(C_5Me_4)(1S,2S,5R$-neomenthyl-$C_5H_3)SmN(TMS)_2$; 2.381 (5) Å calculated, 2.300 (5) Å actual;[55d,e] (*R*)-$Me_2Si(C_5Me_4)$-

(51) (a) Kim, Y.-J.; Osakada, K.; Takenaka, A.; Yamamoto, A. *J. Am. Chem. Soc.* **1990**, *112*, 1096–1104. (b) Osakada, K.; Kim, Y.-J.; Yamamoto, A. *J. Organomet. Chem.* **1990**, *382*, 303–317. (c) Di Bugno, C.; Pasquali, M.; Leoni, P.; Sabatino, P.; Braga, D. *Inorg. Chem.* **1989**, *28*, 1390–1394. (d) Kegley, S. E.; Schaverien, C. J.; Freudenberger, J. H.; Bergman, R. G.; Nolan, S. P.; Hoff, C. D. *J. Am. Chem. Soc.* **1987**, *109*, 6563–6565.

(52) (a) Supplementary material. (b) The first number in parentheses following an averaged value of a bond length or angle is the root-mean-square estimated standard deviation of an individual datum. The second and third numbers, when given, are the maximum deviation from the average value and the number of individual measurements which are included in the average value.

(53) Similarly, the complex $[Ta(Cl)_2(H_2N^tBu)(HN^tBu)(N^tBu)]_2$ has been crystallographically characterized and has a Ta–N(amine) – Ta–N(amido) distance difference of 0.37 Å, and a Ta–N(amido) – Ta–N(imido) distance difference of 0.25 Å. Jones, T. C.; Nielson, A. J.; Rickard, C. E. F. *J. Chem. Soc., Chem. Commun.* **1984**, 205–206.

(54) den Haan, K. H.; de Boer, J. L.; Teuben, J. H.; Spek, A. L.; Kojić-Prodić, B.; Hays, G. R.; Huis, R. *Organometallics* **1986**, *5*, 1726–1733.

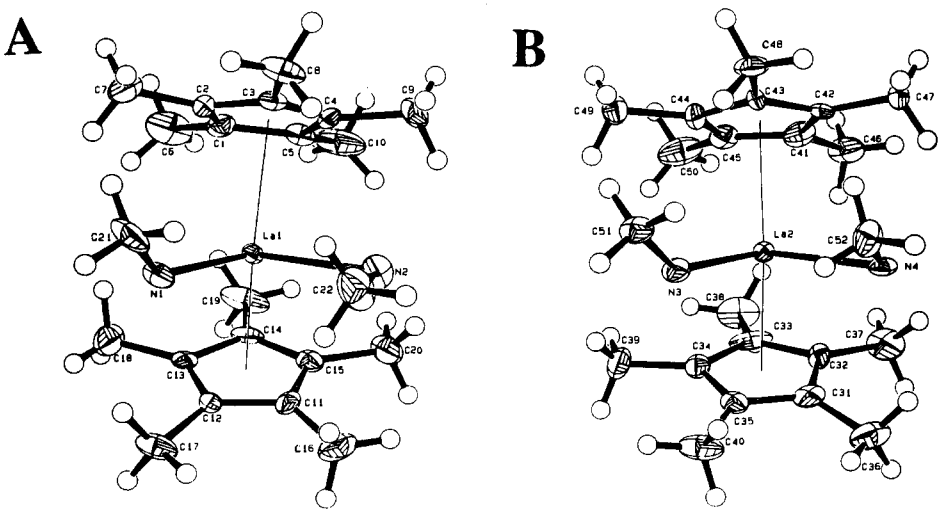

Figure 7. Perspective ORTEP drawing of the crystal structure of $Cp'_2LaNHCH_3(H_2NCH_3)$ (**18**) showing the two crystallographically nonequivalent molecules per unit cell (A and B). All nonhydrogen atoms are represented by thermal ellipsoids drawn to encompass 35% probability.

Table VII. Nonhydrogen Atom Positional Parameters and Estimated Standard Deviations for $Cp'_2LaNHCH_3(H_2NCH_3)$ (**18**)

	x/a	y/b	z/c		x/a	y/b	z/c
La1	0.32961 (3)	0.24826 (6)	0.12095 (3)	La2	0.85864 (3)	0.25786 (6)	0.14675 (3)
N1	0.2643 (5)	0.3014 (9)	0.2027 (5)	N3	0.8049 (5)	0.2268 (8)	0.2390 (5)
N2	0.2555 (6)	0.0607 (8)	0.0810 (6)	N4	0.7751 (5)	0.4330 (8)	0.1043 (5)
C1	0.4690 (6)	0.242 (1)	0.1753 (6)	C31	0.9395 (6)	0.456 (1)	0.1904 (7)
C2	0.4362 (7)	0.197 (1)	0.2247 (7)	C32	0.9735 (6)	0.400 (1)	0.1435 (6)
C3	0.4110 (6)	0.0902 (10)	0.2028 (6)	C33	1.0006 (6)	0.296 (1)	0.1738 (8)
C4	0.4279 (6)	0.0705 (10)	0.1402 (6)	C34	0.9783 (6)	0.2874 (10)	0.2383 (6)
C5	0.4638 (6)	0.162 (1)	0.1192 (7)	C35	0.9419 (6)	0.388 (1)	0.2475 (6)
C6	0.5120 (7)	0.351 (1)	0.1802 (10)	C36	0.9127 (7)	0.578 (1)	0.1830 (8)
C7	0.4325 (8)	0.252 (1)	0.2913 (7)	C37	0.9887 (8)	0.448 (1)	0.0795 (7)
C8	0.3770 (7)	0.005 (1)	0.2456 (7)	C38	1.0530 (7)	0.220 (1)	0.1461 (8)
C9	0.4153 (7)	−0.041 (1)	0.1012 (8)	C39	0.9956 (8)	0.195 (1)	0.2887 (8)
C10	0.5015 (8)	0.165 (2)	0.0600 (8)	C40	0.9133 (7)	0.425 (1)	0.3096 (7)
C11	0.2436 (7)	0.3390 (9)	0.0081 (6)	C41	0.8666 (7)	0.127 (1)	0.0283 (7)
C12	0.2469 (7)	0.4270 (9)	0.0550 (6)	C42	0.7978 (6)	0.1577 (9)	0.0231 (6)
C13	0.3133 (6)	0.4727 (9)	0.0656 (6)	C43	0.7680 (6)	0.0962 (9)	0.0740 (6)
C14	0.3505 (6)	0.410 (1)	0.0226 (6)	C44	0.8198 (7)	0.0290 (10)	0.1097 (6)
C15	0.3079 (7)	0.329 (1)	−0.0129 (6)	C45	0.8811 (7)	0.0471 (10)	0.0808 (7)
C16	0.1793 (7)	0.275 (1)	−0.0176 (8)	C46	0.9172 (8)	0.170 (1)	−0.0159 (7)
C17	0.1880 (7)	0.475 (1)	0.0892 (7)	C47	0.7602 (6)	0.2343 (9)	−0.0278 (6)
C18	0.3429 (8)	0.562 (1)	0.1141 (7)	C48	0.6946 (6)	0.095 (1)	0.0832 (7)
C19	0.4219 (7)	0.441 (1)	0.0100 (8)	C49	0.8135 (7)	−0.054 (1)	0.1655 (6)
C20	0.3248 (8)	0.245 (1)	−0.0646 (6)	C50	0.9470 (7)	−0.017 (1)	0.1006 (9)
C21	0.2499 (7)	0.252 (1)	0.2659 (6)	C51	0.7444 (6)	0.172 (1)	0.2572 (6)
C22	0.2003 (8)	0.045 (1)	0.1191 (9)	C52	0.7068 (7)	0.415 (1)	0.1217 (7)

(1*R*,2*S*,5*R*-menthyl-C_5H_3)$YN(TMS)_2$: 2.42 Å calculated, 2.28 Å actual,[55b,e] $[(CH_3C_5H_4)_2YbNH_2]_2$: 2.49 (1) Å calculated, 2.31 (1) actual),[56] the present La–$NHCH_3$ distances are ~0.1 Å shorter. The La–N bond distance is comparable to those in highly unsaturated single-ring $(C_5Me_5)Ce$ complexes: $Cp'Ce[N(TMS)_2]_2$, 2.370 (4) Å calculated, 2.353 (4) Å actual;[57] $[Cp'Ce(I)N(TMS)_2]_2$, 2.325 (4) Å calculated, 2.308 (4) Å actual.[57] The La–N bond length in **18**, after correction for effective ionic radii,[58] is even slightly shorter than the Hf–N bond length of 2.36 (1) Å, (2.027 (8) Å actual) in $Cp'_2HfNHCH_3(H)$[49d] and the Zr–N bond length of 2.412 Å (2.092 (3) Å actual) in $Cp_2ZrNHPh^+(OTf)^-$,[49i] complexes all suggested to have M–N (M = Zr, Hf) multiple bond character. The present Ln–NH_2R distances are both 2.70 (1) Å and, with suitable ionic radius corrections, are observed to be longer by 0.07–0.1 Å than those in the ammonia complexes of Cp'_2Yb–$XPh(NH_3)$ (X = S, Te; Yb–X calculated, 2.603 (3), 2.63 (1) Å; actual, 2.428 (3), 2.45 (1) Å)[59] and the calculated Yb(II)–N distances of 2.56 (3) Å (2.54 (3) Å actual) and 2.59 (1) Å (2.57 (1) Å actual) for $Cp'_2Yb(THF)(NH_3)$[47] and $Cp'_2Yb(py)_2$,[60] respectively. The large disparity in Ln–N bond distances between amine and amido is in accord with the greatly different bonding environments noted in the ^1H NMR spectra (vide supra).

(55) (a) Using precatalysts such as (*S*)-$Me_2Si(C_5Me_4)$(1*S*,2*S*,5*R*-neomenthyl-C_5H_3)$SmN(TMS)_2$ and (*R*)-$Me_2Si(C_5Me_4)$(1*R*,2*S*,5*R*-menthyl-C_5H_3)$YN(TMS)_2$, which have been characterized by X-ray diffraction, CD spectroscopy, etc., enantioselectivities for the cyclization of **1** and **9** proceed with comparable rates and with ee values as high as 77% at 0 °C.[22b,55b-e] (b) Marks, T. J. *Abstracts of Papers*, 199th National Meeting of the American Chemical Society, Boston, MA, April 22–27, 1990; American Chemical Society: Washington, DC, 1990; CATL14. (c) Gagné, M. R. Ph.D. Thesis, Northwestern University, Evanston, IL, 1991. (d) Conticello, V. P. Ph.D. Thesis, Northwestern University, Evanston, IL, 1990. (e) Gagné, M. R.; Brard, L.; Conticello, V. P.; Giardello, M. A.; Marks, T. J. Submitted for publication.

(56) Hammel, A.; Weidlein, V. *J. Organomet. Chem.* **1990**, *338*, 75–87.

(57) Heeres, H. J.; Meetsma, A.; Teuben, J. H.; Rogers, R. D. *Organometallics* **1989**, *8*, 2637–2646.

(58) The effective ionic radii for eight-coordinate Hf(IV) and Zr(IV) are 0.83 and 0.84 Å, respectively.[43b]

(59) (a) Berg, D. J.; Andersen, R. A.; Zalkin, A. *Organometallics* **1988**, *7*, 1858–1863. (b) Zalkin, A.; Henly, T. J.; Andersen, R. A. *Acta Cyrstallogr., Sect. C: Cryst. Struct. Commun.* **1987**, *C43*, 233.

(60) Tilley, T. D.; Andersen, R. A.; Spencer, B.; Zalkin, A. *Inorg. Chem.* **1982**, *21*, 2647–2649.

Table VIII. Selected Bond Distances (Å) and Angles (deg) for $Cp'_2LaNHCH_3(NH_2CH_3)$ (**18**)

Bond Distances					
La1–N1	2.323 (10)	La1–N2	2.70 (1)	La1–C1	2.84 (1)
La1–C2	2.83 (1)	C1–C2	1.37 (2)	La1–C3	2.83 (1)
C2–C3	1.40 (2)	La1–C4	2.84 (1)	C3–C4	1.37 (2)
La1–C5	2.86 (1)	C1–C5	1.47 (2)	C4–C5	1.38 (2)
C1–C6	1.53 (2)	C2–C7	1.50 (2)	C3–C8	1.53 (2)
C4–C9	1.53 (2)	C5–C10	1.50 (2)	La1–C11	2.86 (1)
C11–C12	1.40 (2)	La1–C13	2.85 (1)	C12–C13	1.42 (2)
La1–C14	2.82 (1)	C13–C14	1.42 (2)	La1–C15	2.84 (1)
C11–C15	1.41 (2)	C14–C15	1.40 (2)	C11–C16	1.51 (2)
C12–C17	1.55 (2)	C13–C18	1.50 (2)	C14–C19	1.52 (2)
C15–C20	1.50 (2)	N1–C21	1.46 (2)	N2–C22	1.44 (2)
La2–N3	2.302 (10)	La2–N4	2.701 (9)	La2–C32	2.84 (1)
C31–C32	1.40 (2)	La2–C33	2.84 (1)	C32–C33	1.43 (2)
La2–C34	2.83 (1)	C33–C34	1.44 (2)	C31–C35	1.40 (2)
C34–C35	1.41 (2)	C31–C36	1.52 (2)	C32–C37	1.48 (2)
C33–C38	1.53 (2)	C34–C39	1.49 (2)	C35–C40	1.51 (2)
La2–C41	2.86 (1)	C41–C42	1.40 (2)	C42–C43	1.45 (2)
La2–C44	2.86 (1)	C43–C44	1.41 (2)	C41–C45	1.42 (2)
C44–C45	1.44 (2)	C41–C46	1.52 (2)	C42–C47	1.49 (2)
C43–C48	1.50 (2)	C44–C49	1.51 (2)	C45–C50	1.51 (2)
N3–C51	1.46 (2)	N4–C52	1.47 (2)	La1–C_g1^a	2.58 (1)
La1–C_g3^a	2.58 (1)	La2–C_g3^a	2.59 (1)	La2–C_g4^a	2.60 (1)
Bond Angles					
N1–La1–N2	95.4 (3)	La1–N1–C21	135.4 (8)	La1–N2–C22	111.6 (8)
N3–La2–N4	92.4 (3)	La2–N3–C51	140.1 (8)	La2–N4–C52	111.4 (7)
C_g1–La1–C_g2^a	136.3 (4)	C_g3–La2–C_g4^a	140.8 (4)		
Torsional Angles					
N1–La1–N2–C22		−0.7 (9)	N4–La2–N3–C51		80 (1)
N3–La2–N4–C52		−32.8 (8)	N2–La1–N1–C21		66 (1)

$^a C_g$ = ring centroid.

The major difference in molecules A and B (Figure 7) lies in the relative orientations of the *N*-methyl groups. In A, the amine methyl group lies in the N–La–N plane (N1–La–N2–C22 dihedral angle = −0.8 (10)°), while the amido methyl is rotated 66 (1)° and 0.94 (1) Å out of the plane (N2–La1–N1–C21 dihedral angle = 66 (1)°). In contrast, both methyl groups are displaced from the N–La–N plane in molecule B such that the amine methyl carbon atom is 0.74 (1) Å above the plane (N3–La2–N4–C52 dihedral angle = −32.6 (8)°) and the amido methyl carbon atom is 0.82 (1) Å above the plane (N4–La2–N3–C51 dihedral angle = 80 (1)°). In comparison, the alkyl groups of $Cp'_2HfNHCH_3(H)$[47d] and $Cp_2ZrNHPh(OTf)$[49i] are rotated 63 (3)° and 74.4° out of the equatorial girdle, respectively. While the present La1–N2–C22 and La2–N4–C52 amine angles are similar (112.3 (9)° and 111.7 (7)°, respectively), the corresponding amido angles differ by ~6° and are opened up to 135.0 (9)° and 141.2 (8)°, respectively. The relatively obtuse La–N–C angles suggest the absence of any La–CH_3 agostic interactions (no La–$C(CH_3)$ distances are less than 3.5 Å) and are slightly smaller than the 145.5 (7)° Hf–N–C angle observed in $Cp'_2Hf-NHCH_3(H)$[49f] and larger than the Zr–N–C angle of 133.4 (3)° observed in $Cp_2ZrNHPh^+(OTf)^-$.[49i] Interestingly, the amine methyl groups of both A and B are oriented toward the ring-centroid–La–ring-centroid plane, opposite to that seen in $Cp_2MoOH(H_2NCH_3)]^+$,[61] a compound proposed to have an intramolecular O–H···N hydrogen bond.

In regard to electronic structure, the 63 (3)° rotation of the NMe group out of the H–Hf–N plane in $Cp'_2HfNHCH_3(H)$ has been attributed to a compromise between the conformation maximizing N lone pair–metal LUMO[62] overlap (O) and that minimizing NMe···MeCp′ nonbonded repulsions (P).[49d] The

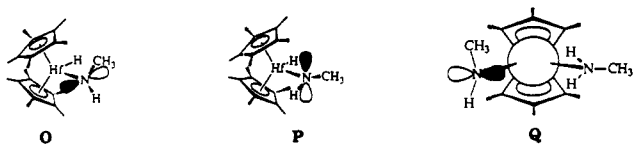

O P Q

upper limit to the Hf–N π-bond strength is ~10 kcal mol^{-1}. Although a similar ligand–LUMO overlap argument could be advanced for **18**, multiple metal–N bonding is on less firm grounds for f-element amides[63,64] (as opposed to alkoxides[65]), and the present NMR data show that the ligand conformations do not lie in deep potential wells. The amido ligand conformation in **18** contrasts with those in $Cp'_2An(Cl)NEt_2$ and $Cp'_2An(NEt_2)_2$ (An = Th, U) where conformation P is implicated by NMR.[21] In addition to possibly optimizing $LaNHCH_3$ π-interactions, it might be argued that the conformation about the La–N bond is associated with hydrogen bonding between the nitrogen lone pair of the amido ligand and the coordinated amine (Q) and/or might offer a low-energy transition state for hydrogen transfer in the amine–amido exchange process. However, the long-observed N–N nonbonded distances in **18** and internal orientation of the coordinated *N*-methylamine preclude such an interaction in the ground state.[66]

Variable-Temperature in Situ NMR Studies of Catalytic Solutions. To assess the stability of the intermediate alkyl complexes proposed in Scheme I, the reaction of $Cp'_2LaCH(TMS)_2$ with a slight excess of various substrates was studied in situ by NMR (eq 20).[67] Generation of the initial lanthanide amido complexes (vide infra) occurs rapidly at −78 °C as in eq 17. Warming and

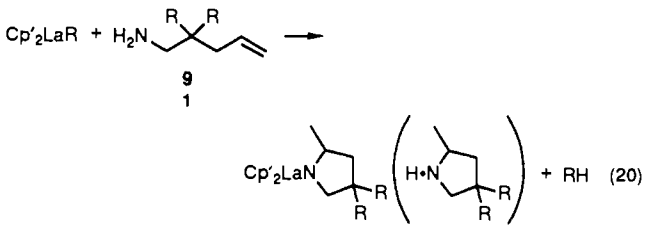

9
1

20, R = CH_3 (52% yield)
21, R = H (44% yield)

stirring at ambient temperature for 12 h ensures complete cyclization in a second step to give monomeric (by cryoscopy in benzene) pentane-soluble complexes, isolable as crystalline materials by slow cooling of pentane solutions (see the Experimental Section for characterization data). ^1H NMR spectra of **20** and **21** reveal an absence of olefinic resonances, indicating complete cyclization. Furthermore, spectral integration indicates that 2 equiv of the cyclized product are present per Cp'_2La unit. That the two 2-methylpyrrolidine units have different chemical environments is further observed in the ^1H-coupled ^{13}C NMR. For **21**, the observation of a quartet of doublets for each of the 2-methylpyrrolidine β-carbon atoms at 0 °C is indicative of the exocyclic methyl group of an amido complex (M), rather than a methylene unit as in a chelating alkyl complex (N), as well as an additional N-coordinated 2-methylpyrrolidine.[68] The obser-

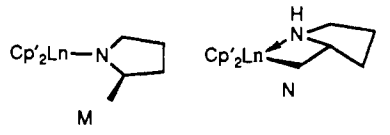

M N

(61) Prout, K.; Cameron, T. S.; Forder, R. A.; Critchley, S. R.; Denton, B.; Rees, G. V. *Acta Crystallogr., Sect. B* **1974**, *30*, 2290–2304.

(62) Lauher, J. W.; Hoffmann, R. *J. Am. Chem. Soc.* **1976**, *98*, 1729–1742.

(63) (a) Bursten, B. E.; Strittmatter, R. J. *Angew. Chem., Int. Ed. Engl.*, in press. (b) Rabaâ, H.; Saillard, J.-Y.; Hoffmann, R. *J. Am. Chem. Soc.* **1986**, *108*, 4327–4333 and references therein.

(64) Raymond, K. N.; Eigenbrot, C. W., Jr. *Acc. Chem. Res.* **1980**, *13*, 276–283.

(65) (a) Bursten, B. E.; Casarin, M.; Ellis, D. E.; Fragalà, I.; Marks, T. J. *Inorg. Chem.* **1986**, *25*, 1257–1261. (b) Duttera, M. R.; Day, V. W.; Marks, T. J. *J. Am. Chem. Soc.* **1986**, *106*, 2907–2912. (c) Cotton, F. A.; Marler, D. O.; Schwotzer, W. *Inorg. Chim. Acta* **1984**, *95*, 207–209.

(66) Typical N–N distances in N···H···N hydrogen bonds are ca. 3.0 Å, with the maximum possible being ~3.5 Å based upon van der Waals radius arguments.[66a] N–N distances are 2.9–3.0 Å for intermolecular N···H···N bonds in early transition metal hydrazido complexes.[66b] (a) Olovsson, I.; Jonsson, P.-G. In *The Hydrogen Bond: Recent Developments in Theory and Experiment*; Shuster, P., Zundel, G., Sandorfy, C., Eds.; North-Holland: Amsterdam, 1976; Vol. II, pp 393–456. (b) Schrock, R. R.; Liu, A. H.; O'Regan, M. B.; Finch, W. C.; Payack, J. F. *Inorg. Chem.* **1988**, *27*, 3574–3583.

(67) Attempted synthesis of **21** using $Cp'_2LaN(TMS)_2$ resulted in substrate cyclization and the recovery of $Cp'_2LaN(TMS)_2$.

vation of a single ν_{NH} stretch in the 3300 cm^{-1} region of the IR spectra (**20**, 3295 cm^{-1} (w); **21**, 3308 cm^{-1} (w); Table VI)[30b] also argues that **20**–**21** are amine–amido complexes.

As in the case of **17**–**19**, **20** and **21** also undergo intramolecular rearrangement that is rapid on the NMR time scale at room temperature. At 0 °C, the ^1H and ^{13}C NMR spectra of **20** and **21** show the presence of one Cp′ and two pyrrolidine ligand environments. At ≥25 °C, broadening of the ^1H amine ligand resonances in **20** and **21** is consistent with amine–amido proton transfer and other dynamic processes (vide infra). The single Cp′ ^1H NMR resonance of **21** remains sharp to ca. −22 °C. Below −22 °C, the signal undergoes broadening and at −44 °C is resolved into two broad envelopes at δ 2.08 and 2.12 ppm, finally sharpening below −55 °C into two sets of two resonances having 1:0.8:0.8:1 intensity ratios (δ 2.16, 2.15, 2.11, and 2.08, respectively). Interpretation of the non-Cp′ ^1H NMR behavior of **21** is not as informative; however, the ^{13}C NMR spectrum at −80 °C clearly shows four Cp′ and four 2-methylpyrrolidine environments. Unlike **21**, the ^1H NMR spectrum of **20** at −70 °C does not exhibit four sets of Cp′ resonances but, instead, one major Cp′ resonance flanked on either side by two minor peaks in a ratio of ~1:6:1 (major δ 2.17; minor δ 2.19, 2.15). At −70 °C, the pyrrolidine resonances are broad with an indication of a major and a minor species. The low-temperature ^{13}C NMR spectrum of **20** shows, in addition to the two sets of pyrrolidine environments seen at 0 °C, an equal number of resonances attributable to a minor isomer. This minor isomer is clearly observable in the ring carbon signals but not in the Cp′ methyl resonances. The structural/dynamic complexities implied by these observations are understandable, considering that the pyrrolyl and pyrrolidine C2 centers are chiral as are the coordinated pyrrolidine NH groups. In addition to the possibility of these four instantaneous diastereomers (*RRR* + *SSS*; *RRS* + *SSR*; *SRR* + *RSS*; *SRS* + *RSR*), it is also possible that rotational isomers exist within the congested metal coordination sphere. In regard to the dynamic processes observed, note that the ligand C2 centers are not inverted by intramolecular proton exchange nor rotation about La–N bonds. Hence, complete averaging of pyrrolyl/pyrrolidine and diastereomeric/diastereotopic Cp′ resonances can only occur via rapid *intermolecular* heterocyclic ligand exchange.

When solutions of $Cp'_2LaCH(TMS)_2$ are treated with 2 equiv of substrates **5** and **9** and kept at low temperature, the amine–amido products exhibit dynamic NMR behavior similar to that observed for the $Cp'_2LaNHR(H_2NR)$ model complexes. Thus, at −60 °C, the ^1H NMR spectrum of the compound formed with **9** shows two complete sets of amino olefin proton resonances. The chemical shift differences of the amido and amine protons are rather striking, with $\Delta\delta \approx 0.50$ ppm observed for the remote C4 olefinic resonances (δ 5.48 and 6.02) (Figure 8A). Differences ranging from 0.15 to 1.25 ppm are observed for the remainder of the amine–amido signals. On increasing the temperature to −33 °C, all peaks begin to broaden. Further broadening continues to −22 °C, at which point substrate cyclization begins to complicate the spectra. At this temperature, however, the two sets of olefinic C5 resonances (δ 5.05 and 5.20 at −60 °C) have coalesced. Most other pairs differ more in resonance frequency and are not yet coalesced at this temperature. The $\Delta G^{\ddagger}$ for this process is calculated to be 12.2 ± 0.5 kcal mol^{-1} (at −20 °C),[50] similar to that observed for $Cp'_2LaNHR(H_2NR)$ model complexes (vide supra). Exchange in the amine–amido complex formed from **5** occurs with $\Delta G^{\ddagger}$ = 12.3 ± 0,5 kcal mol^{-1} (at −20 °C).[50]

In situ monitoring of solutions containing higher concentrations of **5** and **9** reveals only one set of amino olefin resonances at room temperature. That up to three sets of substrate resonances, corresponding to Ln–NHR, Ln←H_2NR, and free amine, are expected indicates that a dynamic process or combination of processes gives rise to global exchange of amine environments. To further probe this behavior, variable-temperature ^1H NMR

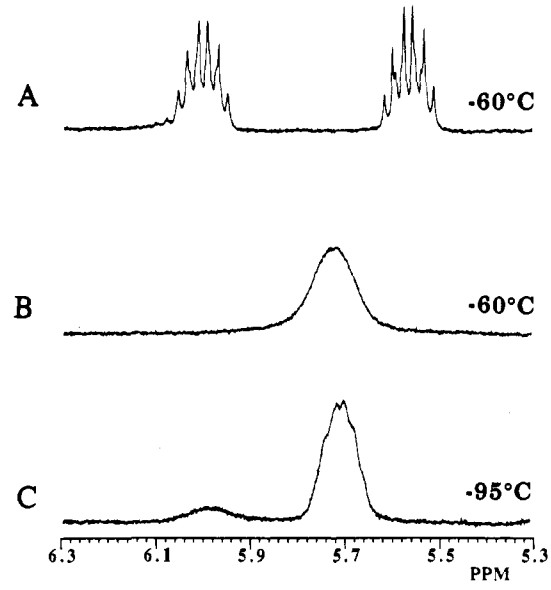

Figure 8. Variable-temperature ^1H NMR spectra in toluene-d_8 in the vinylic region. A, $Cp'_2LaCH(TMS)_2$ + 2 equiv of $H_2NCH_2CMe_2CH_2CH{=}CH_2$ (**9**) at −60 °C; B, $Cp'_2LaCH(TMS)_2$ + 8 equiv of **9** at −60 °C; C, $Cp'_2LaCHTMS_2$ + 8 equiv of **9** at −95 °C.

experiments were conducted with a dilute (~1.2 mM) $Cp'_2LaCH(TMS)_2$ solution containing 8 equiv of **9**. At −95 °C, the olefinic region displays two sets of olefinic resonances in a ratio of ~1:7 (Figure 8C). The chemical shift of the minor $CH{=}CH_2$ resonance (δ 6.03) corresponds to one of the signals observed in the previously discussed case with 2 equiv of **9** (Figure 8A). The major peak is located at δ 5.75, similar to that observed at room temperature in the presence of a large excess of **9**. Interestingly, the second vinylic CH resonance observed in the 2-equiv experiment (δ 5.48) is not observed in Figure 8C. Upon warming the solution to −80 °C, the minor peak shifts upfield and becomes a broad shoulder on the major peak at 5.75 ppm. A further increase in temperature to −60 °C (Figure 8B) averages the two resonances and suggests the rapid exchange of all amine environments. It appears, therefore, that addition of excess amine not only accelerates the amine–amido H-transfer process (compare Figures 8A,B) but that even at −95 °C the free amine is rapidly exchanging with coordinated amine. Although the bound/free amine exchange is facile at −95 °C, it appears that the catalyst retains an acentric environment as indicated by the presence of equal-intensity Cp′ signals at δ 2.15 and 2.08. At 25 °C, the two Cp′ environments are in rapid exchange. A 20 mM solution of $Cp'_2LaCH(TMS)_2$ with 7 equiv of **5** shows similar amine–amido exchange behavior, with the exception that slowing of the dynamic exchange can be observed at ca. −40 °C rather than −95 °C as in the case of **9**. Continued cooling does not allow the observation of separate free and coordinated amine resonances, suggesting that as with **9** base exchange is facile at −95 °C. A similar inter/intramolecular exchange process involving bound and free HOR has been identified in $(PMe_3)_3RhOR(HOR)$ complexes (eq 19). In this case, exchange of free and bound HOR is rapid at −80 °C by ^1H NMR, and exchange between alkoxide and free/bound alcohol is slow at temperatures below 45 °C.[51d] Above 45 °C, global averaging of alkoxide and free/bound alcohol is observed, analogous to the present organolanthanide case with amines.

Using paramagnetic catalyst precursors such as $Cp'_2SmCH(TMS)_2$ and $Cp'_2NdCH(TMS)_2$, it can be established that the aforementioned free–coordinated amine exchange process does not include the secondary heterocyclic cyclization products. Thus, significant broadening and chemical shift displacements are only observed in substrate ^1H NMR signals, resulting from interaction with the paramagnetic center. In contrast, the product resonances remain sharp and unshifted, arguing that once cyclized, the 2-methyl heterocycles do not effectively compete with substrate for

(68) For a lanthanide alkylamine complex, see: van den Hende, J. R.; Hessen, B.; Meetsma, A.; Teuben, J. H. *Organometallics* **1990**, *9*, 537–539.

the catalyst center nor function as inhibitors during typical catalytic reaction conditions.

Discussion

Hydroamination and Catalyst Scope. The hydroamination/cyclization results in Table II illustrate the wide range of substrate structures that undergo catalytic cyclization to products, including 5-, 6-, and 7-membered heterocycles as well as primary, secondary, and aromatic amines. Preparative-scale reactions have been carried out on scales approaching 2 g of substrate and 30 mg of catalyst. General reactivity trends with metal size and ancillary ligation (Tables IV and V) suggest that high levels of coordinative unsaturation are required for efficient heterocycle synthesis.

The $Cp'_2LnN(TMS)_2$ class of complexes serve as readily synthesized catalyst precursors. As observed in the case of **9** + $Cp'_2LaN(TMS)_2$, the lower reactivity of the $NTMS_2$ complexes toward bulky substrates gives rise to a slight induction period. Compared to the more easily synthesized $Cp'_2Sm(THF)_2$ precursor,[37a] the amide route allows the catalytically more active lighter lanthanide precursors to be accessed. In cases where high catalytic activity is not crucial, $Cp'_2Sm(THF)_2$ prepared in one synthetic step also serves as a convenient precursor. For the purpose of this study, the short induction period (<5 s at −78 °C) and high activity of the diamagnetic $Cp'_2LaCH(TMS)_2$ precatalyst renders it the reagent of choice.

Mechanism. Product Regioselectivities and Rates of Cyclization. A priori, two isomers are possible for each cyclized product. In the case of **2** (entry 1 in Table II), these regioisomers are the 5-*exo*, R (2-methylpyrrolidine), and the 6-*endo*, S (piperidine), products. Both isomers are favorable based on the Baldwin rules for ring closure and are observed in group 10-centered stoichiometric hydroamination/cyclization processes.[69,70] In the present organolanthanide systems, molecular models suggest that severe bond length and angle distortions are incurred in the olefin insertion transition state (vide infra) affording the 6-*endo* product, and the exo product (R) is thus favored. In addition, R may be kinetically favored in a transition state having a positively charged β-carbon atom (T).[71,72] Experimentally, in situ ^1H NMR and GC/MS studies indicate the exclusive formation (>99%) of the *exo*-methyl product in all cases. The present efficacy in cyclizing **3** → **4** and even 7-membered rings (**15** → **16**) is in direct contrast to the known stoichiometric Pd and Pt chemistry, where cyclization to 6-membered heterocycles is either very difficult or impossible.[12,24b] Additionally, these latter processes do not exhibit the high regioselectivities observed in the organolanthanide-catalyzed process.

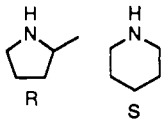

R S

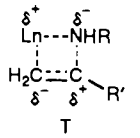

T

Suggestive of turnover-limiting ring formation is the wide variation of cyclization rates with substrate architecture (Table II). Thus, skeletal methyl substitution of 1-aminopent-4-ene (**1**) increases the rate of cyclization dramatically (**5** → **6**, **7** → **8**, **9** → **10**), while 2-aminohex-5-ene (**3** → **4**) undergoes cyclization ~30 times more slowly than 1-aminopent-4-ene (**1** → **2**). These changes in amino olefin structure would not be expected to significantly alter the rate of proton transfer (ii, Scheme I) but should significantly affect the rate of olefin insertion/cyclization (i, Scheme I). The dramatic rate enhancement in entry **5** is an example of the classic Thorpe–Ingold effect[73] of *gem*-dimethyl groups on cyclization, resulting from nonbonded interactions in the acyclic form relative to the cyclic. Since the relative rates (i.e., **5** > **6** ≫ **7**)[74] reflect trends expected for sterically controlled ring-forming transition states, they support a turnover-limiting olefin insertion mechanism. For example, the present substituent effects on cyclization rates parallel the observed cyclization reactivities of substituted amino-4-bromobutenes (eq 21).[75] Additionally, the relative ordering of catalyst activities with metal size and ancillary ligation (Tables IV and V), as will be discussed below, is similar to that observed for other sterically controlled, lanthanide-centered olefin insertion processes.[15] The relative rates, stereoselectivities, and parallels to similar heterocycle-forming reactions thus suggest that the present catalysis proceeds via a turnover-limiting, ring-forming olefin insertion step.

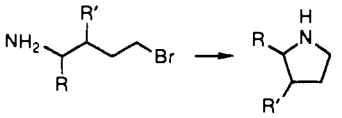

(21)

Mechanism. Metal Ion Size and Ancillary Ligation Effects. Catalytic activity dependencies on metal ion size have previously been observed in other Cp'_2Ln-catalyzed processes. Turnover frequencies for ethylene polymerization are metal size dependent, with $N_1 \geq 1450\ s^{-1}$ for Ln = La and $N_1 = 100\ s^{-1}$ for Ln = Lu.[15b] Similar are Cp'_2Ln-catalyzed cyclohexene hydrogenation rates, which have a turnover-limiting olefin insertion step and follow the general order, La > Nd > Sm > Lu.[15d] For Cp'_2Ln catalysts, the aforementioned catalytic turnover frequencies span approximately one order of magnitude, from the largest La^{3+} ion (radius = 1.160 Å)[43] to the smallest Lu^{3+} ion (eight-coordinate ionic radius = 0.977 Å), while the present catalytic system shows a change of $\sim 10^3$ from $La^{3+} \rightarrow Lu^{3+}$ (Table IV), arguing for a sterically demanding transition state in the turnover-limiting step.

Attempts to increase the reactivities of lanthanide Cp'_2 compounds led to the design of chelating ancillary ligands, such as $Me_2SiCp''_2$,[44] where the centroid–metal–centroid angle is decreased from ~134° to ~122°.[15b,c] This increased unsaturation is manifested in an order of magnitude increase in propylene oligomerization activity by the corresponding organolanthanide complexes,[15a-d] as well as a 10^3 rate increase in 1-hexene hydrogenation activity by $(Me_2SiCp''_2ThH_2)_2$ over $(Cp'_2ThH_2)_2$.[44] That $Me_2SiCp''_2LuCH(TMS)_2$-catalyzed hydroamination/cyclization rates increase relative to the unbridged ligand system presumably reflects the more open coordination environment (N_1 increases for **9** → **10** from <1 h^{-1} (80 °C) to 75 h^{-1} (80 °C; Table V)). Entries 6 and 8 of Table II show that this ancillary ligand is also efficacious in mediating sterically demanding transformations such as the cyclization of secondary amines and the formation of 7-membered heterocycles. The $Et_2SiCpCp''$ ligand offers further opening of the lanthanide coordination sphere,[28] and Table V shows that this ligation is accompanied by a further increase in the **9** → **10** cyclization rate (N_1 = 200 h^{-1} at 80 °C). Interestingly, lanthanide $Et_2SiCpCp''$ complexes are ineffective olefin hydrogenation catalysts because the hydrides undergo a rapid, deactivating ligand redistribution.[28] The present efficacy in olefin hydroamination is consistent with Scheme I (or variants thereof), which does not involve hydride intermediates. Taken together, the pronounced lanthanide ion size and ancillary ligand effects on hydroamination/cyclization rates argue for a sterically rather sensitive olefin insertion transition state.

(69) Pd- and Pt-catalyzed cyclizations give mixtures of endo and exo heterocycles.[12b,d,e]

(70) March, J. *Advanced Organic Chemistry*; 3rd ed.; John Wiley & Sons: New York, 1985; p 187.

(71) Lin, Z.; Marks, T. J. *J. Am. Chem. Soc.* **1990**, *112*, 5515–5525.

(72) In some cases, destabilizing substituents may direct olefin insertion to proceed via a sterically less favorable pathway: Guram, A. S.; Jordan, R. F. *Organometallics* **1990**, *9*, 2190–2192.

(73) Kirby, A. J. *Adv. Phys. Org. Chem.* **1980**, *17*, 183–278.

(74) For the cyclization of $Br(CH_2)_xCO_2^-$, the following relative rates are observed as a function of ring size: 3, 21.7; 4, 5.4 × 10^3; 5, 1.5 × 10^6; 6, 1.7 × 10^4; 7, 97.3; 8, 1.00.[74a] (a) Reference 70, pp 185–186. (b) DeTar, D. F.; Luthra, N. P. *J. Am. Chem. Soc.* **1980**, *102*, 4505–4512. (c) Mandolini, L. *J. Am. Chem. Soc.* **1978**, *100*, 550–554.

(75) Brown, R. F.; van Gulik, N. M. *J. Org. Chem.* **1956**, *21*, 1046–1049.

Scheme II. Mechanistic Scenarios

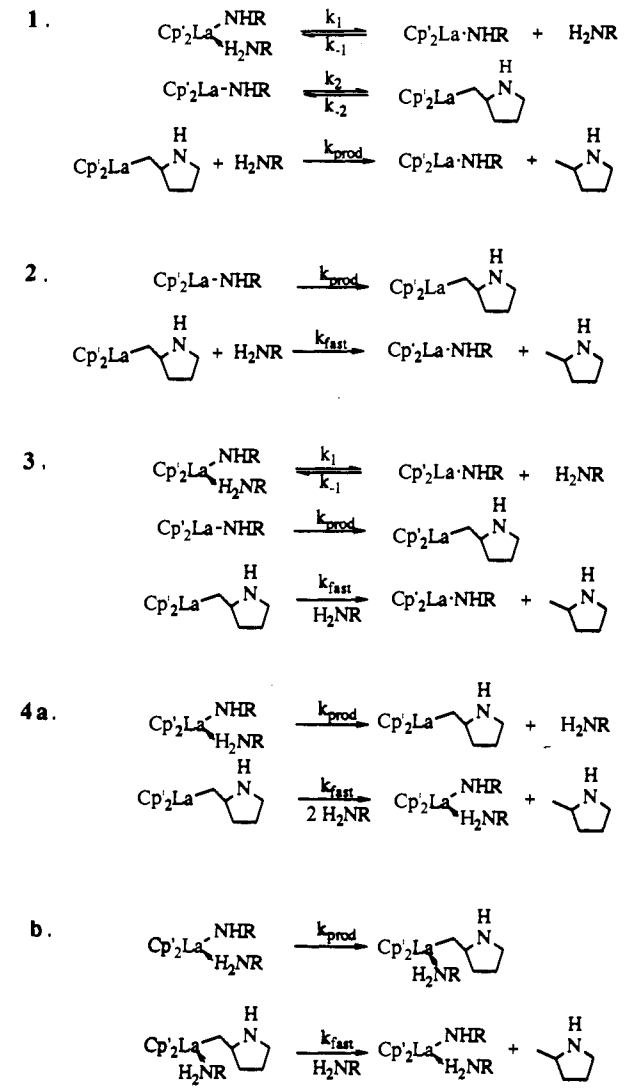

Mechanism. The Possibility of Radical Processes. While the possibility that the amino olefin hydroamination/cyclization process is partially or completely radical (chain) in nature (e.g., eqs 22 and 23) appears remote, the opposing evidence warrants brief summation. Thus, the present substrate architecture, metal

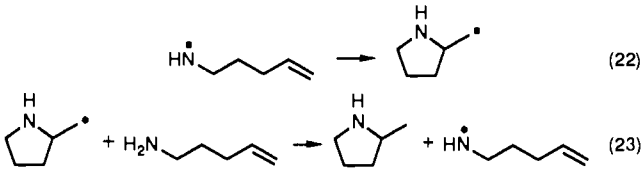

(22)

(23)

ion size, and ancillary ligand effects on turnover frequency, regioselectivity, diastereoselectivity, and enantioselectivity[55] as well as large turnover numbers are in marked contrast to the phenomenology observed in radical amino olefin cyclization processes.[76,77] Moreover, the present trends in rate correlate well with those of classical nonradical cyclizations and other lanthanide-centered olefin transformations[15a-d] rather than with metal redox couples.[78,79] These arguments lead us to discount the significance of radical processes.

Mechanism. Cyclization Kinetic Analysis. The four most reasonable mechanistic scenarios (elaborations of Scheme I) for hydroamination/cyclization are shown in Scheme II. They are as follows: (1) fast, reversible olefin insertion followed by turnover-limiting protonolysis; (2) base-free catalyst with turnover-limiting olefin insertion; (3) base-free catalyst in equilibrium with a base adduct (turnover-limiting olefin insertion); and (4) (a) concerted amine displacement from an amine–amido complex with turnover-limiting olefin insertion or (b) permanent amine coordination during turnover-limiting olefin insertion. It will be seen that several of these can be convincingly rejected on the basis of kinetic and other data.

Scenario 1 involves rapid, reversible amine binding and olefin insertion, coupled to a turnover-limiting protonolysis of the lanthanide alkyl (which rationalizes the observed NH/ND kinetic isotope effects). Assuming steady-state concentrations of the olefin-inserted catalytic intermediate, the rate expression for this process is given by eq 24:[80,81a]

$$\text{velocity} = \frac{k_{\text{prod}}k_2k_1[\text{LnN}_2]}{(k_{-1}(k_{-2} + k_{\text{prod}}[\text{S}]))} \qquad (24)$$

in which [S] and [LnN_2] are the substrate and amine–amido concentrations, respectively. Under rapid equilibrium conditions (i.e., $k_{\text{prod}}[\text{S}] \ll k_{-2}$) zero-order behavior in substrate is predicted.[81a] Although this is consistent with the observed rate law, a number of mechanistic observations are inconsistent with the approximation used to generate it. No evidence exists, for example, for a reversible olefin insertion process, since (i) *trans*-2,5-dimethylpyrrolidine is not isomerized by the Cp'_2La catalyst, and (ii) when chiral π-ancillary ligands ($Me_2Si(Me_4C_5)(R^*C_5H_3)Ln$-) are used, ee's as high as 77% are observed for the cyclization of **1** and **9** (i.e., k_{-2} would seem to be very small).[22b,55] Furthermore, protonolysis of lanthanide alkyls by amines is both rapid and irreversible as demonstrated by the aforementioned low-temperature ^{1}H NMR experiments, indicating quantitative protonolysis of sterically encumbered $Cp'_2LnCH(TMS)_2$ by amines at −78 °C to generate free $CH_2(TMS)_2$ and the catalytically active $Cp'_2LnNHR(H_2NR)$ complexes. For Ln = Nd and Sm, instantaneous color changes observed upon addition of amines at −78 °C also indicate the rapidity of the facile process. If protonolysis of a 100 mM $Cp'_2LnCH(TMS)_2$ solution occurs in 5 s at −78 °C, then the Eyring plot in Figure 1B predicts a turnover frequency of $\sim 1 \times 10^7$ h^{-1} for a turnover-limiting protonolysis at 20 °C, 5–6 orders of magnitude greater than the observed catalytic rates. These rate discrepancies and data implicating irreversible olefin insertion in fact suggest that $k_{\text{prod}} \gg k_2$ and that $k_{-2} \ll k_{\text{prod}}$. The above mechanistic results, therefore, imply that $k_{-2} \ll k_{\text{prod}}[\text{S}]$, and scenario 1 should display inverse first-order behavior in substrate, which is incompatible with the observed kinetic data.

Scenario 2 involves a base-free lanthanide amido complex undergoing a turnover-limiting olefin insertion. Analysis by standard kinetic methods[80] yields the rate expression, velocity =

(76) Newcomb, M.; Burchill, M. T.; Deab, T. M. *J. Am. Chem. Soc.* **1988**, *110*, 6528–6535 and references therein.

(77) Cyclization of 2-aminohexene aminyl radicals yields trans:cis ratios of 2,5-dimethylpyrrolidines ranging from ~3:1 to all cis-containing products, depending on the radical source (chemical or electrochemical). (a) Newcomb, M.; Marquardt, D. J.; Deeb, T. M. *Tetrahedron* **1990**, *46*, 2329–2344. (b) Tokuda, M.; Yamada, Y.; Takagi, T.; Suginome, H.; Furusaki, A. *Tetrahedron* **1987**, *43*, 281–296.

(78) Morss, L. R. *Chem. Rev.* **1976**, *76*, 827–841.

(79) For examples of lanthanide (Eu^{II},Sm^{II})-initiated radical processes, see: (a) Finke, R. G.; Keenan, S. R.; Schiraldi, D. A.; Watson, P. L. *Organometallics* **1987**, *6*, 1356–1358. (b) Finke, R. G.; Keenan, S. R.; Schiraldi, D. A.; Watson, P. L. *Organometallics* **1986**, *5*, 598–601.

(80) (a) Moore, J. W.; Pearson, R. G. *Kinetics and Mechanisms*, 3rd ed.; Wiley: New York, 1981; pp 313–317 and references therein. (b) Segel, I. H. *Enzyme Kinetics*; Wiley: New York, 1975; Chapters 1–3.

(81) (a) The equilibrium approximation for scenario 1 in Scheme II gives

$$\text{velocity} = \frac{k_{\text{prod}}k_1k_2\ [\text{LnN}_2]}{k_{-1}k_{-2}}$$

(b) The equilibrium approximation for scenario 3 in Scheme II gives

$$\text{velocity} = \frac{k_{\text{prod}}k_1\ [\text{LnN}_2]}{k_{-1}[\text{S}]}$$

k_{prod}[LnNHR], where [LnNHR] is the concentration of the amido catalyst. This rate law adequately predicts the zero-order kinetics in substrate, but variable-temperature ^{1}H NMR, elemental analysis, conversion-dependent diastereoselectivities, X-ray diffraction results, and kinetic isotope effect arguments (vide infra) implicate amine coordination to the Lewis acidic metal in both the catalyst resting and transition states, arguing that 2 is also not the predominant pathway.

Scenario 3 takes into account the propensity of Cp'_2LnNHR species to bind additional Lewis bases. In this scenario, the amine adduct is in rapid preequilibrium with a base-free form, the precursor to turnover-limiting olefin insertion. Kinetic analysis using standard steady-state conditions in Cp'_2LnNHR[80,81b] yields the rate law of eq 25, in which [S] and [LnN_2] are the substrate and amine–amido concentrations, respectively. Since k_{prod} is

$$\text{velocity} = \frac{k_{prod}k_1[LnN_2]}{k_{-1}[S] + k_{prod}} \qquad (25)$$

expected to be less than k_{-1}[S], this rate law suggests that the reaction should show self-inhibition (i.e., the velocity should increase with decreasing substrate concentration), contrary to experimental observations. Additional evidence which suggests that cyclization does not occur from the base-free form is found in the aforementioned exogenous amine-sensitive diastereoselectivities in the cyclization of (*R,S*)-**5** and in kinetic isotope effect arguments (vide infra), which also implicate amine coordination in the transition state.

On the basis of the above discussion, two alternative mechanistic schemes can be proposed which account for all of the aforementioned information. Scenarios 4a and 4b both invoke bound amine in the immediate coordination environment of the olefin insertion transition state, thereby providing the necessary circumstances for amine-influenced diastereoselection and, as will be seen, kinetic isotope effects in the cyclizations of $\mathbf{1d_2}$, $\mathbf{5d_2}$, and $\mathbf{9d_2}$. The two pathways differ in the disposition of the amine following turnover-limiting insertion. Scenario 4a is the case in which amine is displaced concurrent with olefin insertion. For this process to show no substrate self-inhibition, the insertion/amine displacement step must be irreversible (which is reasonable and consistent with the previously discussed integrity of *trans*-**6** in the presence of Cp'_2La and the high ee's observed for cyclization of **1** and **9** by chiral catalysts).[55] Equally consistent is mechanism 4b, in which amine remains coordinated throughout the olefin insertion process. Although 4b appears to be disfavored on steric grounds, 4a and 4b cannot be rigorously distinguished on the basis of the aforementioned data. However, additional insights are provided by NH/ND kinetic isotope effects, as well as by the temperature dependence of the cyclization process.

Mechanism. Kinetic Isotope Effects. Substantial kinetic isotope effects (KIEs) for the cyclizations of $\mathbf{1d_2}$, $\mathbf{5d_2}$, and $\mathbf{9d_2}$ (eqs 14–16), are detected. For the cyclization of $\mathbf{1d_2}$, $\mathbf{5d_2}$, and $\mathbf{9d_2}$, the turnover frequencies N_t (h^{-1}) are 52 (60 °C), 8.8 (25 °C), and 23 (25 °C), yielding KIEs of 2.7 (4) (60 °C), 5.2 (8) (25 °C), and 4.1 (8) (25 °C), respectively. These KIEs are independent of both substrate and catalyst concentration as well as conversion (Figure 2). In light of the substantial evidence supporting turnover-limiting olefin insertion, the magnitudes of the present KIEs are somewhat surprising since no NH/ND bonds need to be formed or broken in a simple olefin insertion into a Ln–N bond. However, the measured NH/ND effects are significant compared to the maximum theoretical[82] KIE of ~9.0 (25 °C), based on a ν_{NH} of 3300 cm^{-1}, and are highly suggestive of a primary effect.[82] For α-NH abstraction processes at group 4 centers (eq 26), primary KIEs of 5.9 (6) (90 °C, M = Ti) to 7.3 (4) (90 °C, M = Zr) have been reported.[83] Proton-transfer processes exhibit a wide variety

$$(^tBu_3SiNH)_3MCH_3 \xrightarrow[\Delta]{-CH_4} (^tBu_3SiNH)_2M{=}NSi^tBu_3 \qquad (26)$$

Scheme III. Possible Sources of the NH/ND Kinetic Isotope Effect

a. Ln-C Protonolysis in the Transition State

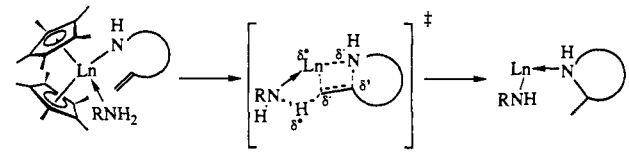

b. Amine-Assisted Amido Insertion

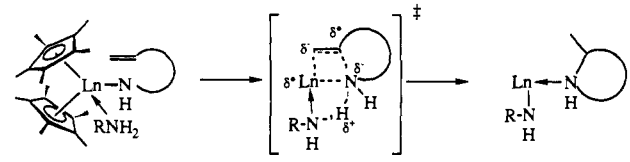

of KIEs depending on solvent, acid, and base sources, but they usually range from 2.5 to 7.0 for oxygen-based acids.[82] The present KIEs are of an unprecedented magnitude for secondary isotope effects[84] (as might arise from a hybridization change or "agostic" interactions[85] involving the LnNHR group undergoing insertion[86]) and would require what appears to be a physically unrealistic combination of force constant changes.

Since evidence for a turnover-limiting olefin insertion is so compelling, the NH/ND KIE cannot reasonably derive from a discrete, turnover-limiting protonolysis of a previously formed Ln–C bond. However, alternative explanations are suggested by examining how a coordinated amine might stabilize the olefin insertion transition state. Such considerations lead to two reasonable sources of the KIE (Scheme III). The first and perhaps most likely source (Scheme IIIa) involves the transfer of a proton from a coordinated amine to the partially polarized α-carbon in the 4-membered insertion transition state. Such a transfer would stabilize the negative charge buildup, in essence protonolyzing the Ln–C bond as it was being formed and ensuring an irreversible insertion. In such a transfer, the proton would be delivered at a relatively obtuse angle and account for the significant KIE. The mechanism shown in Scheme IIIb is similar to IIIa, where charge buildup in the transition state, in this case at nitrogen, is stabilized by a hydrogen bond from the coordinated amine (rapid subsequent proton migration would yield the product shown). Mechanism IIIb constrains olefin insertion from the lateral direction (external to the two bound N atoms), while Scheme IIIa directs olefin approach via a central (between the N atoms) insertion trajectory. Molecular modelling analysis of the approach of norbornene toward the U–H bond of $Cp'_2UH(OR^*)$ (R* = [(1*S*)-*endo*]-bornoxide) for insertion (U) reveals the pathway which bisects the H–U–O angle to be highly favored over the trajectory in which the olefin approaches from the lateral direction.[71] Additionally, product absolute stereochemistries arising from the asymmetric catalytic hydrogenation of 2-phenyl-1-butene by chiral $R_2Si(Me_4C_5)(R^*C_5H_3)LnH$ complexes (R* = (1*S*,2*S*,5*R*)-neomenthyl, (1*R*,2*S*,5*R*)-menthyl, and (1*R*,2*S*,5*R*)-8-phenylmenthyl) can be rationalized in terms of a similar central approach of the olefin to the metal hydride.[55b,d,87] If similar approach trajectories are

(82) (a) Bell, R. P. *The Proton in Chemistry*, 2nd ed.; Cornell University Press: Ithaca, NY, 1973; Chapter 12. (b) Melander, L.; Saunders, W. H., Jr. *Reaction Rates of Isotopic Molecules*; Wiley: New York, 1980.

(83) (a) Cummins, C. C.; Schaller, C. P.; Van Duyne, G. D.; Wolczanski, P. T.; Dith Chan, A. W.; Hoffmann, R. *J. Am. Chem. Soc.* **1991**, *113*, 2985–2994. (b) Cummins, C. C.; Baxter, S. M.; Wolczanski, P. T. *J. Am. Chem. Soc.* **1988**, *110*, 8731–8733.

(84) (a) Ritchie, C. D. *Physical Organic Chemistry*; Marcel Dekker: New York, 1990; Chapter 8. (b) Carpenter, B. K. *Determination of Organic Reaction Mechanisms*; Wiley: New York, 1984; Chapter 5.3.

(85) (a) Piers, W. E.; Bercaw, J. E. *J. Am. Chem. Soc.* **1990**, *112*, 9406–9407. (b) Krauledat, H.; Brintzinger, H.-H. *Angew. Chem., Int. Ed. Engl.* **1990**, *29*, 1412–1413. (c) Clawson, L.; Soto, J.; Buchwald, S. L.; Steigerwald, M. L.; Grubbs, R. H. *J. Am. Chem. Soc.* **1985**, *107*, 3377–3378.

(86) For an example of an "agostic" Pt···H–N interaction, see: Hedden, D.; Roundhill, D. M.; Fultz, W. C.; Rheingold, A. L. *Organometallics* **1986**, *5*, 336–343.

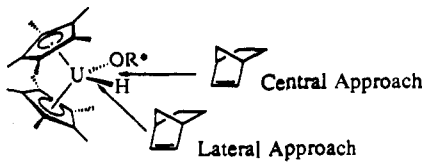

U

applicable to the hydroamination/cyclization insertion step, then the KIE source shown in Scheme IIIa should be favored over that shown in Scheme IIIb.

Mechanism. Activation Parameters. The activation parameters for the present proposed turnover-limiting insertion transition state appear to be typical of the highly organized, polar transition states of d^0, f^n-centered transformations. The modest $\Delta H^{\ddagger}$ value (12.7 (1.4) kcal mol^{-1}) suggests a concerted transition state with significant bond making to compensate for the bond breaking. The large, negative $\Delta S^{\ddagger}$ value (−27 (5) eu) is consistent with a highly organized, polar transition state (e.g., pseudobicyclic[85a,c] [2.0.3] V) in which significant loss of internal rotational degrees of freedom has occurred. In simple S_N2 heterocyclic ring-closures,

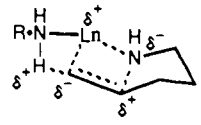

V

$\Delta S^{\ddagger}$ is typically ca. −5 to −17 eu for 5- and 6-membered rings.[74b,c] Similar $\Delta S^{\ddagger}$ values are observed in Cp'_2ThR_2-centered cyclometalation processes (eq 27; $\Delta S^{\ddagger}$ = −10 to −24 eu) which are believed to proceed via analogous cyclic transition states (W).[88]

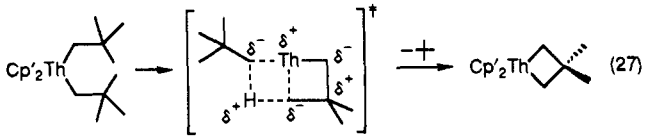

W

Mechanism. Kinetic Effects of Exogenous Bases. As noted above, the addition of noncyclizable Lewis bases (e.g., THF, *n*-propylamine) has the effect of slowing the reaction rate and qualitatively altering the kinetic order in substrate concentration toward first-order (Figure 4). This behavior is consistent with competition between the substrate and the inhibitory (nonproductive substrate) Lewis base for the catalytic center and is reminiscent of a classical enzymatic kinetic inhibition scenario with the provisos that little free enzyme is present (K_m is very small) and that species other than "E·S" and "E·I" may be present (vide infra). Scheme IVa follows Scheme IIa,b and depicts the simplest conceivable scenario. A standard rapid equilibrium analysis[80b] yields eq 28

$$\text{velocity} = \frac{[\text{Ln}_{\text{tot}}]k}{1 + \dfrac{K[\text{I}]}{[\text{S}]}} \qquad (28)$$

where $[\text{Ln}_{\text{tot}}]$ = total lanthanide concentration, S = substrate, and I = Lewis base inhibitor. This relationship reduces to the observed zero-order in [S] kinetics for [I] = 0 and predicts that $1/v$ vs $1/[\text{S}]$ plots ("reciprocal" plots)[80b] should yield families of radiating straight lines for different values of [I] (Figure 9A). Moreover, replots of the above slopes vs [I][80b] should yield a straight line with zero intercept at [I] = 0. Plots of the kinetic data of Figure

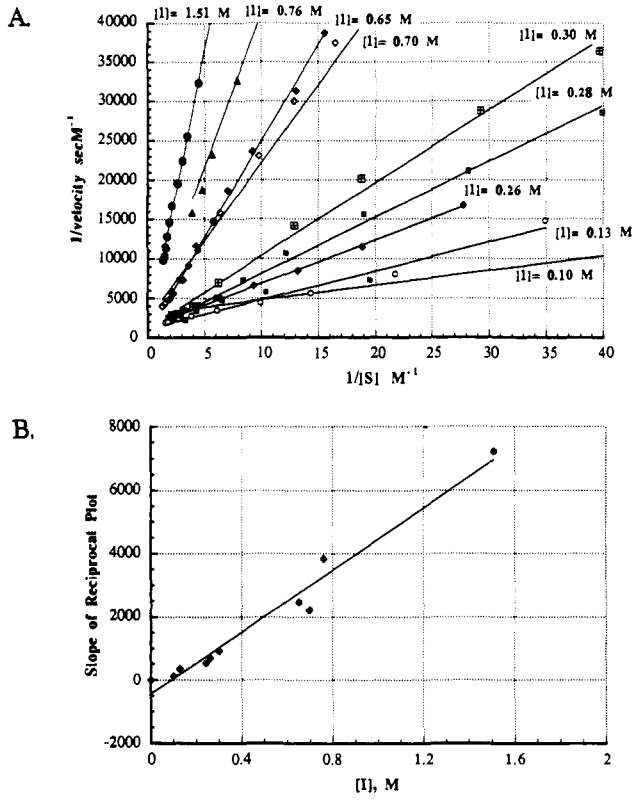

Figure 9. A. Reciprocal kinetic plot (1/velocity vs 1/[substrate]) for the hydroamination/cyclization of $H_2NCH_2CMe_2CH_2CH{=}CH_2$ (**9**) using $Cp'_2LaCH(TMS)_2$ as the precatalyst in the presence of varying amounts of the inhibitor (I) *n*-propylamine, modelled by Scheme IVa and eq 26. The lines are linear least-squares plots through the data points. B. Plot of the slopes of the lines in Figure 9A versus *n*-propylamine concentration.

Scheme IV. Models for Lewis Base Kinetic Inhibition[a]

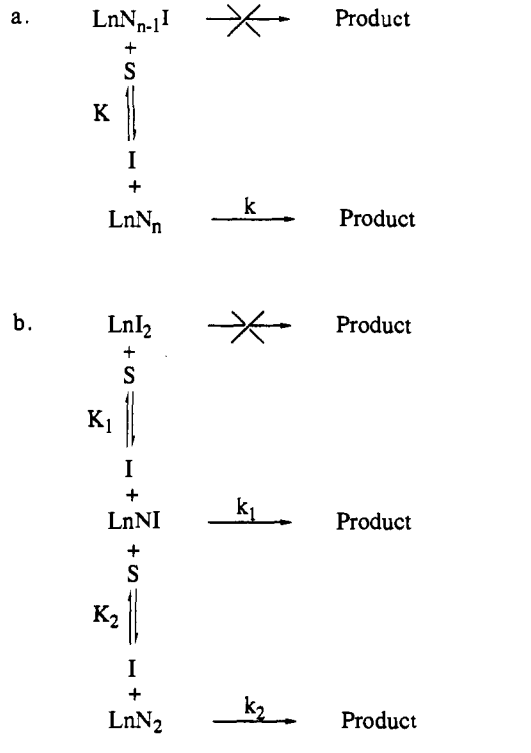

[a] I = inhibitor, N = bound substrate (amine or amido), S = free substrate.

4B give reasonable qualitative adherence to this admittedly simplified model, as shown in Figure 9.[89] Scheme IVb presents a

(87) Brard, L.; Conticello, V. P.; Giardello, M. A.; Tsuji, Y.; Stern, C. L.; Marks, T. J. Manuscript in preparation.

(88) (a) Smith, G. M.; Carpenter, J. D.; Marks, T. J. *J. Am. Chem. Soc.* **1986**, *108*, 6805–6807. (b) Bruno, J. W.; Smith, G. M.; Marks, T. J.; Fair, C. K.; Schultz, A. J.; Williams, J. M. *J. Am. Chem. Soc.* **1986**, *108*, 40–56.

Scheme V. Diastereoselection in the Cyclization of 2-Aminohex-5-ene

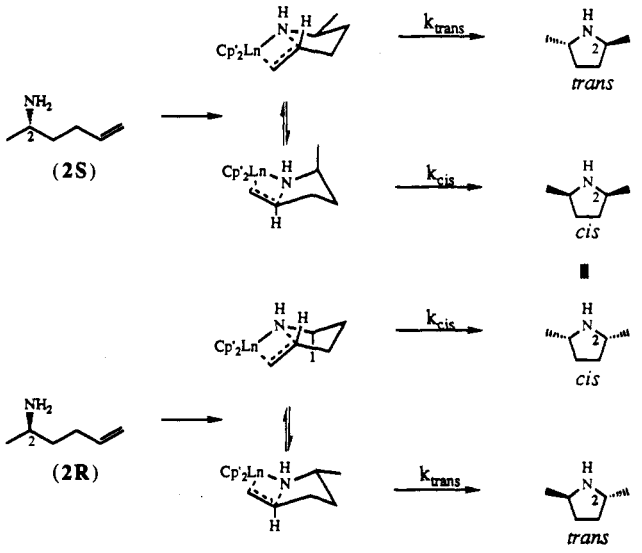

more elaborate and realistic kinetic description and leads to eq 29, assuming rapid equilibrium conditions. This expression

$$\text{velocity} = \frac{[\text{Ln}_{\text{tot}}]\left(k_2 + k_1K_2\dfrac{[\text{I}]}{[\text{S}]}\right)}{1 + K_2\dfrac{[\text{I}]}{[\text{S}]} + K_1K_2\left(\dfrac{[\text{I}]}{[\text{S}]}\right)^2} \qquad (29)$$

contains four unknown, independent constants (k_1, k_2, K_1, K_2), of which only one, k_2, can be independently determined. Attempts to measure K_1 and K_2 by NMR or spectrophotometry have so far been unsuccessful. It can be seen for [I] = 0 that eq 29 reduces to uninhibited, zero-order kinetics and, for [I] = large, to velocity $\sim$[S]/[I] (as expected). For k_1 and K_1 small, eq 29 reduces to eq 28. By setting $k_2 = 2.6 \times 10^{-2}$ s^{-1} (the measured value) and using nonlinear regression techniques, fits to eq 29 converge (for a wide range of independent input parameters) to $K_1 = 1.8$ (0.2), $K_2 = 10$ (14), and $k_1 = 0.04$ (0.02) s^{-1}. While the ordering $K_2 > K_1$ is consistent with steric expectations and k_1 is of a reasonable magnitude, we are reluctant to ascribe any more than qualitative significance to these results in support of Scheme IVb. Nevertheless, both these first and second levels of analysis strongly argue that the effect of exogenous Lewis bases is to depress the observed rate of turnover by competing for and blocking sites at the catalyst center.

Mechanism. Diastereoselection in the Formation of 2,5-Dimethylpyrrolidine. As noted above, diastereoselection in the **5** → **6** cyclization (eq 10) is remarkably sensitive to a variety of factors, including ancillary ligation, lanthanide ionic radius, exogenous bases (Table III), extent of conversion, isotopic substitution (Figure 3A), and initial substrate concentration (Figure 3B). In contrast, diastereoselection in the corresponding cyclization of 2-methyl-1-aminopent-4-ene (eq 11, **7** → **8**) exhibits little sensitivity to these factors. At the initial level of analysis, these results can be understood on the basis of steric/conformational effects in a cyclic 7-membered chair transition state for olefin insertion (Scheme V),[85a,c,90] Thus, nonbonded interactions arising from congestion in the metal coordination sphere (e.g., binding of additional bases; vide infra) should destabilize the sterically more demanding axial methyl conformation and favor the trans product. In the case of **7** → **8**, the methyl substituent is one position further removed from the metal center in the cyclic transition state (to C2), and diastereoselection is expected to be far less sterically sensitive (as observed).

In regard to the conversion dependence of diasteroselection in **5** → **6** (which exhibits zero-order kinetics in substrate over 4 half-lives), the origin of this effect cannot be simply explained via Scheme V. As written, favoring one channel over the other in this scheme effects no obvious diastereoselection but rather a kinetic resolution, the origin of which is not obvious for an achiral catalyst and which is not observed experimentally. Rather, it should be recognized that the "resting state" of the catalyst consists of amine–amido complexes that, for chiral substrate **5**, will consist (in the presence of rapid intramolecular proton exchange) of diastereomeric *R,R* + *S,S* and (interconverting) *RS*/*SR* pairs. Admitting the possibility of additional amine coordination (vide infra) increases the possible number of diastereomers to four (*RRR* + *SSS*,*RRS* + *SSR*,*SRR* + *RSS*,*SRS* + *RSR*, assuming rapid interligand proton exchange). The source of the conversion (substrate concentration) dependent diastereoselection could then be attributed to either of two effects. Differences in the dissociation constants of diastereomeric amine–amido pairs, reasonably having different diastereoselectivities in the **5** → **6** transformation, would lead to conversion dependence of the relative populations. Such a scenario of course invokes significant dissociation of the amine–amido complex (Y in eq 30) which has not been observed experimentally (vide supra). Moreover, the origin of the con-

$$\underset{\text{X}}{\text{Cp}'_2\text{Ln(NHR)(NH}_2\text{R)}_2} \rightleftarrows \text{NH}_2\text{R} + \underset{\text{Y}}{\text{Cp}'_2\text{Ln(NHR)(NH}_2\text{R)}} \rightleftarrows \underset{\text{Y}}{\text{Cp}'_2\text{Ln(NHR)}} + \text{NH}_2\text{R} \qquad (30)$$

version-independent kinetic isotope effect cannot be explained, since a neighboring ligand is no longer available in Y as a proton source (Scheme III). More appealing is an analogous population dependence on conversion arising from the population of one or more diastereomeric diamine–amido structures at high substrate concentrations (X in eq 30). This scenario explains the conversion-independent kinetic isotope effect and is consistent with a picture in which increased congestion at the metal center (i.e., at high substrate concentrations or in the presence of more compact exogenous bases) favors a trans-rich product (Scheme V). This scenario is of course constrained by the observation of a conversion-independent turnover frequency (Figure 3A), indicating that the turnover frequencies through the two or more product-forming channels are nearly equal although the diastereoselectivities are not. Attempts to unambiguously observe species X spectrophotometrically have so far been unsuccessful.[91]

The effects of NH_2 deuteration on the **5** → **6** transformation are pronounced (Figure 3A). In common with the protioamine cyclization, the rate of total *cis*-**6** + *trans*-**6** product formation in the deuterated system is zero-order in substrate. It can also be seen in Figure 3A that there is a substantial kinetic isotope effect (5.2 (8)) on the overall rate of *cis*-**6** + *trans*-**6** formation at 25 °C. Closer inspection of the individual diastereomer data clearly indicates a KIE for *trans*-**6** formation and probably also one for *cis*-**6** formation (judging from the higher conversion data where protio *cis*-**6** quantities are sufficient to measure accurately). However, the deuterated amine cyclization exhibits two additional features: (i) there is no detectable conversion dependence of diastereoselection, and (ii) there is little diastereoselectivity. One possible interpretation of i is that eq 30 exhibits a nonnegligible equilibrium isotope effect that forces the cyclization largely through a single reaction channel. Without a detailed knowledge of the structure of X and attendant vibrational characteristics, the effect of $NH_2 \rightarrow ND_2$ substitution on eq 30 is difficult to predict.[84a,92] It is conceivable that deuteration might enhance

(89) Deviations from straight-line plots in Figure 9A and from a zero intercept in Figure 9B may reflect both the inadequacy of the kinetic model as well as experimental inaccuracies due to difficulties in anaerobically measuring out small quantities of reagents.

(90) (a) Rigollier, P.; Young, J. R.; Fowley, L. A.; Stille, J. R. *J. Am. Chem. Soc.* **1990**, *112*, 9441–9442. (b) Young, J. R.; Stille, J. R. *Organometallics* **1990**, *9*, 3022–3025.

(91) The position of equilibrium 28 is also likely to vary with lanthanide ion size and steric encumbrance.

(92) Wolff, W. In *The Hydrogen Bond*; Schuster, P., Zundel, G., Sandorfy, C., Eds.; North Holland: Amsterdam, 1976; Chapter 26.

Scheme VI. Mechanistic Scheme for Hydroamination/Cyclization

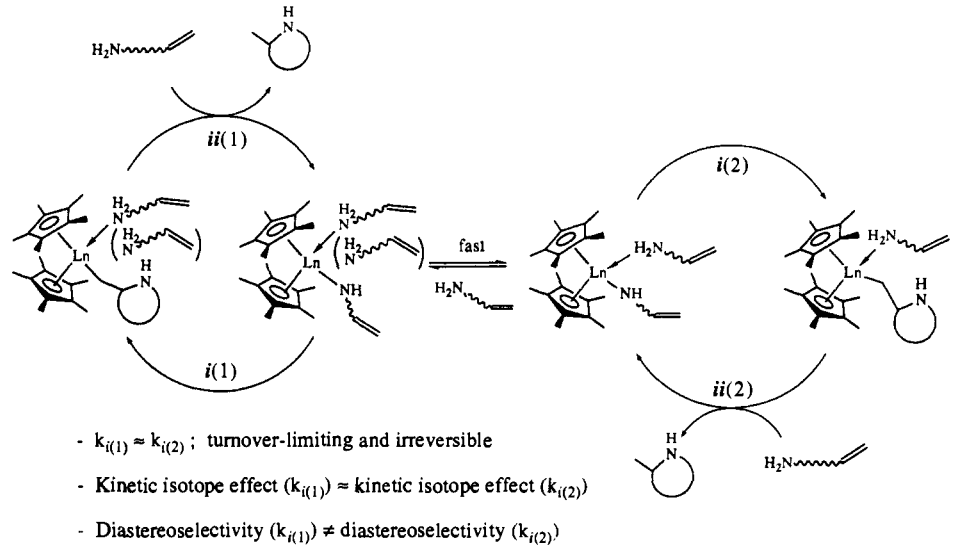

hydrogen bonding in a structure such as Z,[84a,92] thus stabilizing the precursor to trans-rich product. While this conjecture explains

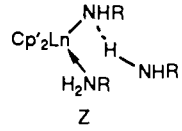

Z

the conversion independence of diastereoselection via a single reaction channel[93] model, it does not alone explain the low diastereoselectivity. That is, if *cis*-**6** and *trans*-**6** formation exhibited identical KIEs in a particular reaction channel, the data in Figure 3A would argue that significant **5** → **6** diastereoselection should be observed (as appears to be the case for both protio reaction channels; Figure 3A). The observed behavior suggests instead that cis/trans branching within a given reaction channel is isotope-dependent, i.e., *cis*-**6** and *trans*-**6** formation proceeds with different KIEs, with the equilibration of the cyclic conformations in Scheme V being more rapid than heterocyclic ring closure (this equilibration could also exhibit an isotope effect although it is difficult to see why the magnitude should be large). While additional experiments will clearly be required to fully elucidate the nature of this isotope effect, it is apparent from the present information that N–H bond breaking is an intimate part of the hydroamination/cyclization transition state and that **5** → **6** diastereoselection is not irrevocably fixed prior to this event.

Mechanistic Recapitulation. In formulating a concluding hydroamination/cyclization scheme which encompasses all of the mechanistic observations, it is useful to briefly summarize the results.

(i) Lanthanide ion size and ancillary ligand effects on rates parallel those of other olefin insertion processes.

(ii) Substrate sensitivity of rates parallels classical cyclization processes.

(iii) Kinetics are zero-order in substrate over a wide concentration and conversion range.

(iv) $\Delta H^{\ddagger}$ and $\Delta S^{\ddagger}$ values suggest a highly organized transition state.

(v) RNH_2/RND_2 experiments establish regiospecific (irreversible) delivery of a single D to a β-C position and reveal primary KIEs of 2.7–5.2.

(vi) Diastereoselection in 2,5-dimethylpyrrolidine formation is sensitive to conversion, initial substrate concentration, added Lewis bases, and $NH_2 \rightarrow ND_2$ substitution.

(vii) Negligible racemization of chiral products at long reaction times and high ee's observed with chiral catalysts indicate that cyclization is essentially irreversible.

(viii) Ln–alkyl + H_2NR protonolysis processes are extremely rapid compared to reaction turnover frequencies.

(ix) At low substrate concentrations, the predominant form of the catalyst is an amine–amido complex in which rapid proton interchange permutes these ligands. Rapid exchange with free substrate but not free product also occurs.

Observations i–iv, vii, and viii argue for irreversible, intramolecular olefin insertion as the turnover-limiting step. Observations v, vi, and ix argue that variable numbers of amine ligands are coordinated to the catalytic center and that these significantly modulate the stereochemistry of the ring-closure process but influence rates mainly via competition with substrate molecules for the reaction centers. The dual manifold scenario shown in Scheme VI presently provides the chemically/structurally most reasonable accommodation of these facts. It invokes comparable cyclization rate constants and overall kinetic isotope effects in the two manifolds but differing diastereoselectivities of ring closure where applicable.

Further research will focus on additional aspects of the scope and selectivity of catalytic hydroamination/cyclization processes as well as on extensions to other heteroatoms.

Acknowledgment. We are grateful to the NSF for support of this research under Grants CHE-8800813 and CHE-9104112. M.R.G. thanks Rhône-Poulenc for a graduate fellowship. We also thank Prof. A. G. M. Barrett for suggestions regarding several organic syntheses and Dr. C. Sishta for assistance with the CPMAS NMR experiments.

Supplementary Material Available: Tables of positional and anisotropic thermal parameters and full tables of bond distances, angles, and dihedral angles for **18** (8 pages); tables of observed and calculated structure factors from the final cycle of least-squares refinement (36 pages). Ordering information is given on any current masthead page.

(93) An alternative explanation of conversion-independent diastereoselection would be that one reaction channel had a far larger KIE than the other, thus allowing little product formation via the slower pathway. Since the observed KIE is 5.2 (8), the unknown, higher KIE would have to be rather large—perhaps unrealistically so.[84]